

2. EXPLANATORY NOTES¹

Shipboard Scientific Party²

INTRODUCTION

In this chapter, we have assembled information that documents our scientific methods. This information concerns only shipboard methods described in the site reports making up the Leg 172 *Initial Reports* volume of the Ocean Drilling Program (ODP). Methods for shore-based analyses of Leg 172 data will be described in the individual scientific contributions to be published in scientific journals and in the *Scientific Results* volume. Coring techniques and core handling, including the numbering of sites, holes, cores, sections, and samples, were the same as those reported in previous *ODP Initial Reports* volumes (e.g., Sigurdsson, Leckie, Acton, et al., 1997)

Authorship of Site Chapters

The entire volume should be treated as a publication contributed by the scientists listed at the front of this volume. Each scientist, however, had one or more areas in which he/she was one of the primary contributors. These are listed below (authors are listed in alphabetical order; no seniority is implied):

Principal Results: Keigwin, Rio
Background and Objectives: Keigwin, Rio
Operations: Acton, Rourt
Lithostratigraphy: Bianchi, Flood, Franz, Hagen, Haskell, Horowitz, Reuer, Yokokawa
Biostratigraphy: Chaisson, Cortijo, Poli, Raffi, Winter
Paleomagnetism: Acton, Clement, Lund, Okada, Williams
Stratigraphic Correlation: Flood
Sedimentation and Mass Accumulation Rates: Chaisson, Cortijo, Ternois
Geochemistry: Borowski, Çagatay, Ternois
Physical Properties: Dunbar, Giosan, Grütznér, Laine
Downhole Logging: Williams
Site Geophysics: Acton, Flood, Laine

Shipboard Scientific Procedures

Numbering of Sites, Holes, Cores, and Samples

For all ODP drill sites, a letter suffix distinguishes each hole drilled at the same site. For example, the first hole drilled is assigned the site number modified by the suffix "A," the second hole takes the site number and suffix "B," and so forth. The cored interval is measured in meters below seafloor (mbsf). The depth below seafloor is determined by subtracting the water depth estimated from the initial drill pipe measurement, which gives the length of pipe from the rig floor to the seafloor (measured in meters below rig floor, mbrf), from the total drill pipe measurement. Each cored interval is generally 9.5 m long, which is the length of a core barrel. Coring intervals may be shorter and may not necessarily be adjacent if separated by drilled intervals.

A recovered core is divided into 1.5-m sections that are numbered serially from the top. When full recovery is obtained, the sections are numbered from 1 through 7, with the last section possibly being shorter than 1.5 m (rarely, an unusually long core may require more than seven sections). When less than full recovery is obtained, there will be as many sections as needed to accommodate the length of the core recovered. By convention, material recovered from the core catcher of a sedimentary core is placed in a separate section during the core description, labeled core catcher (CC), and placed below the last section recovered in the liner. The core catcher is placed at the top of the cored interval in cases where material is only recovered in the core catcher.

When the recovered core is shorter than the cored interval, the top of the core is equated with the top of the cored interval, by convention, to achieve consistency in handling analytical data derived from the cores. Samples removed from the cores are designated by distance measured in centimeters from the top of the section to the top and bottom of each sample removed from that section. A full identification number for a sample consists of the following information: leg, site, hole, core number, core type, section number, piece number (for hard rock), and interval in centimeters measured from the top of the section. For example, a sample identification of "172-1063A-3H-1, 10–12 cm" would be interpreted as representing a sample removed from the interval between 10 and 12 cm below the top of Section 1 in Core 3H of Hole 1063A from Leg 172.

All ODP core identifiers indicate core type. The following abbreviations are used: H = hydraulic piston core (HPC; also referred to as APC, or advanced hydraulic piston core); X = extended core barrel (XCB); and M = miscellaneous material.

Core Handling

Sediments

As soon as a core is retrieved on deck, it goes through a sequence of processing steps. First, a sample is taken from the core catcher and given to the paleontological laboratory for an initial age assignment. The core is then placed on the long horizontal rack, and gas samples may be taken by piercing the core liner and withdrawing gas into a vacuum tube (Vacutainer). Voids within the core are sought as sites for gas sampling. Next, the core is marked into section lengths, each section is labeled, and the core is cut into sections. Interstitial water, (IW) whole-round samples, and headspace gas samples are then taken as a matter of ODP policy (typically on every third core). After initial IW and Vacutainer gas samples were collected, many small holes were drilled into the core liners for most of the cores from Leg 172 to allow gas to escape.

Each section is then sealed at the top and bottom by gluing on color-coded plastic caps—blue to identify the top of a section and clear for the bottom. A yellow cap is placed on the section ends from which a whole-round sample has been removed, and the sample code (e.g., IW) is written on the yellow cap. The caps are usually attached to the liner by coating the end liner and the inside rim of the cap with acetone, and then the caps are taped to the liners. The core sections are then carried into the laboratory, where the individual sections are again labeled using an engraver to permanently mark the full design-

¹Keigwin, L.D., Rio, D., Acton, G.D., et al., 1998. *Proc. ODP, Init. Repts.*, 172: College Station, TX (Ocean Drilling Program).

²Shipboard Scientific Party is given in the list preceding the Table of Contents.

nation of the section. The length of the core in each section and the core-catcher sample are measured to the nearest centimeter; this information is logged into the shipboard JANUS database program.

Cores of soft material are split lengthwise into working and archive halves. The softer cores are split with a wire or saw, depending on the degree of induration. Harder cores are split with a band saw or diamond saw. The wire-cut cores are split from the bottom to top, so investigators should be aware that older material could have been transported up the core on the split face of each section. Following the initial scientific measurements, both halves of the core are put into labeled plastic tubes, sealed, and transferred to cold-storage space aboard the drilling vessel. At the end of Leg 172, the cores were transferred from the ship in refrigerated air freight containers to cold storage at the ODP Core Repository in Bremen, Germany.

JANUS Database

On Leg 172, much of the shipboard data was entered into JANUS, an ORACLE-based database system. Data entered into the JANUS system include core/section depth, voids, multisensor track (MST) data (GRAPE [gamma-ray attenuation porosity evaluator], magnetic susceptibility, *P*-wave logger [PWL], and gamma ray), discrete physical property and chemical measurements, and biostratigraphic data. Data not entered into the JANUS system onboard include paleomagnetic data and color reflectance.

LITHOSTRATIGRAPHY

This section outlines the procedures conducted to document the basic sedimentology for cores collected during ODP Leg 172, including core descriptions, smear slides, color reflectance, and X-ray diffraction. This section is intentionally structured to present only general procedure overviews and departures from ODP conventions. Reference should be made to the “Explanatory Notes” chapters of the ODP *Initial Reports* volumes for Legs 162 (Shipboard Scientific Party, 1996a), 164 (Shipboard Scientific Party, 1996b), and 171B (Shipboard Scientific Party, 1998), which covered similar sedimentary environments and served as a basis for Leg 172 procedures.

Visual Core Description and Barrel Sheets

Visual core descriptions (available from ODP) were made for individual sections and then transcribed into the AppleCORE software package (version 0.7.5b, 1989–1996), customized for Leg 172 to generate barrel sheet summaries for each core. The barrel sheets are presented with core photographs in Section 4 of this volume.

Lithology

Sediment lithologies are presented on the barrel sheets in the “Lithology” column using the symbol set shown in Figure 1. Relatively homogeneous mixtures of various components comprise much of the sediment, and as many as three major constituents are represented graphically, separated by vertical columns. In a few cases, four sediment components were present, making it necessary to combine similar components (e.g., silt and clay as “silty clay”). These instances were noted. Thinly interbedded sediments (millimeter-to-centimeter scale) are unusual and are noted as accessory symbols. Only intervals thicker than 20 cm can be clearly resolved on the graphical representation of the lithologic column, even though smaller units may be present in the core.

At Sites 1062, 1063, and 1064, diatoms, radiolarians, silicoflagellates, and sponge spicules were regarded as a biogenic silica class and not just individual components as at previous sites. With this approach, biogenic silica became a lithologically significant category

and were introduced into the lithology as of Site 1062 using the “diatom ooze” or “mixed biosiliceous ooze” symbols for the summed biosiliceous components.

Sedimentary Structures, Accessories, and Bioturbation Intensity

A key to the symbols used to denote sedimentary structures, accessories, and core disturbances is given in Figure 1. Sedimentary structures are listed as “Physical Structures” on the barrel sheet. The “Accessories” column includes fossil components as well as other special features.

Relative bioturbation activity is shown in the “Bioturbation Intensity” column and divided into three levels of intensity (shown by shades of gray, with darkest being most intense):

1. Low/none; primary sedimentary structures are largely intact, with no signs of mottled sediment.
2. Moderate; bioturbation is visible as discrete structures. Primary sedimentary structures are only moderately disrupted.
3. High; several generations of bioturbation structures are overprinted on each other. There is almost total disruption of sedimentary structures resulting in nearly homogeneous sediment. In this case, however, it may be difficult to distinguish an absence of structures because of bioturbation from the actual absence of primary structures.

Core Disturbance

Observation of sediment disturbance related to the coring process is illustrated in the “Core Disturbance” column on the core description form by the symbols shown in Figure 1. The disturbance categories used were the same as those used during earlier ODP cruises (e.g., Shipboard Scientific Party, 1996a).

Samples

The positions of samples taken from each core for shipboard analysis are indicated in the “Samples” column on the barrel sheet using the following notation:

GEO = location of inorganic and organic carbon analysis;
 IW = location of whole-round interstitial water geochemistry analysis;
 PAL = location of paleontology sample;
 PH = location of close-up photograph;
 SS = location of smear-slide sample;
 T = location of thin-section sample; and
 XRD = location of samples for X-ray diffraction.

Smear-Slide Summary

Tables that summarize the data from smear slides are presented in Section 5, respectively (CD-ROM, back pocket, this volume). Relative abundance of different grain types was made on a semi-quantitative basis (Rothwell, 1989), primarily targeting lithologic classification. Abundances were assigned using the following system:

N or blank = none (not present);
 T = trace (0%–2%);
 R = rare (2%–10%);
 C = common (10%–25%);
 A = abundant (25%–50%); and
 D = dominant (>50%).

The subjective nature of these data should be kept in mind. This is particularly the case where the fine-grained nature of the sediment

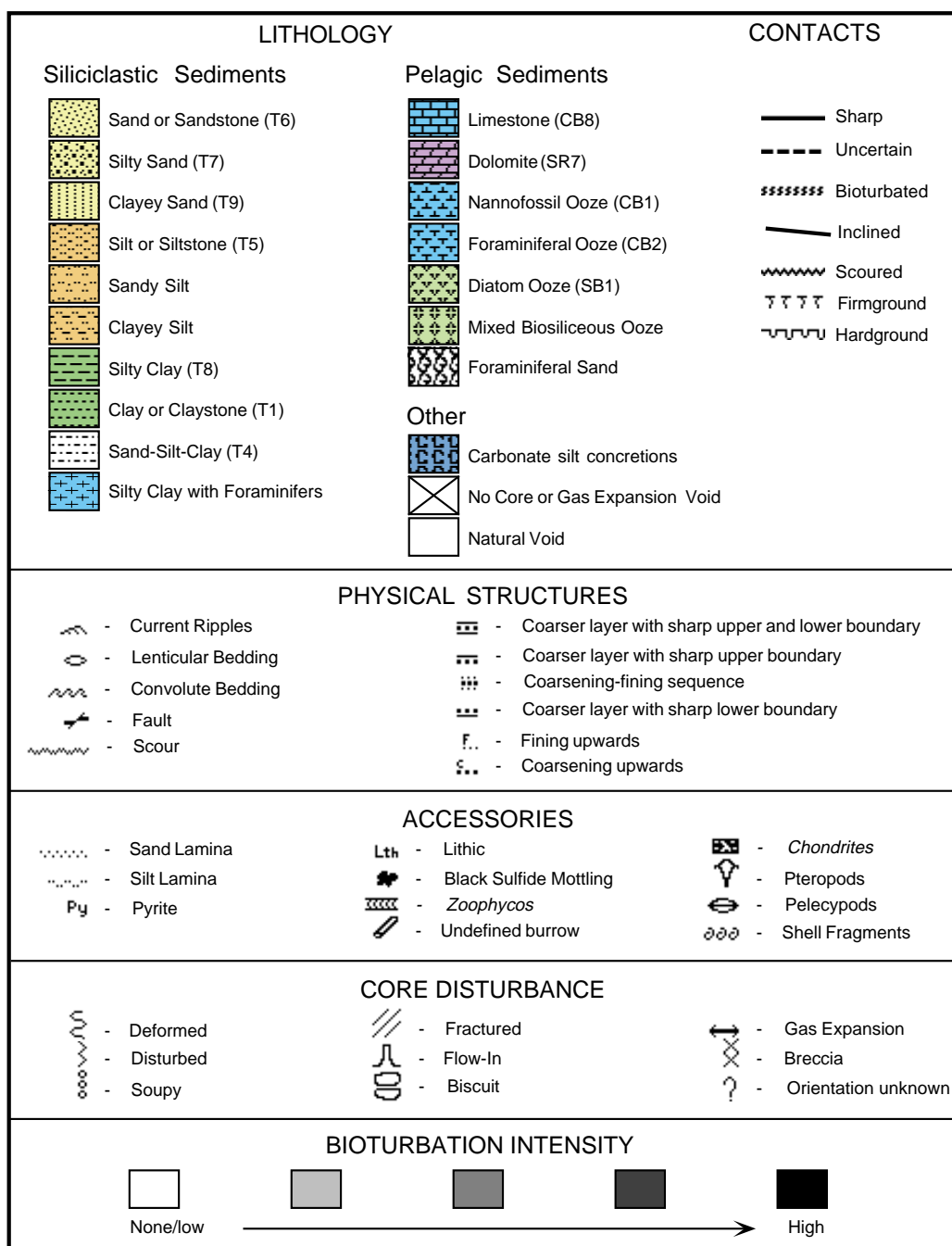


Figure 1. Lithology, accessory, bioturbation, and disturbance symbols used in the barrel sheets.

made it difficult to assess nannofossil content. In some cases, mineralogy from smear-slide estimates could be validated by carbonate analyses (see “Geochemistry” section, this chapter) and/or X-ray diffraction (XRD).

Color

Core color for the visual descriptions was made with Munsell soil color charts (Munsell, 1975). On the barrel sheets, the colors are presented with the terminology presented in Table 1. A much more detailed core analysis is presented in the color reflectance data (see “Color Reflectance” section, this chapter).

Classification of Sediments and Sedimentary Rocks

A slightly modified version of the ODP sediment classification scheme (Mazullo et al., 1988) was used during Leg 172 for granular sediments following the one outlined in the ODP Leg 162 “Explanatory Notes” chapter (Shipboard Scientific Party, 1996a). Leg 172 sediments are subdivided into three groups, depending upon the relative proportion of the pelagic and siliciclastic end-members. It is likely that some biogenic material was transported, but this was difficult to distinguish, and all biogenic components were therefore regarded as pelagic.

During core description, lithologies were largely assigned on the basis of color, and subtle lithologic variations (e.g., biogenic silica

Table 1. Codes for sediment colors used in the barrel sheets.

Intensity		Modifier		Color	
Abbreviation	Meaning	Abbreviation	Meaning	Abbreviation	Meaning
vlt	Very light	bl	Bluish	BK	Black
lt	Light	br	Brownish	BL	Blue
mlt	Medium light	cr	Creamy	CR	Cream
med	Moderate	gy	Greyish	GY	Grey
mdk	Medium dark	gn	Greenish	GN	Green
dk	Dark	or	Orange	OR	Orange
vdk	Very dark	ol	Olive	OL	Olive
vpl	Very pale	pk	Pinkish	PK	Pink
pal	Pale	pu	Purplish	PU	Purple
dsk	Dusky	rd	Reddish	RD	Red
vds	Very dusky	wh	Whitish	WH	White
bri	Brilliant	ye	Yellowish	YE	Yellow
viv	Vivid	mo	Mottled	BF	Buff
str	Strong	sp	Spotty		
dp	Deep				
vdp	Very deep				

content) may have remained undetected. Lithologies were periodically verified with smear slides, but slight differences in the sediment composition at the precise location where the smear-slide samples were taken may lead to small variations in the lithology assigned to stratigraphically equivalent units from different holes. General correlations nevertheless remain consistent.

Principal Names

Sediment classification uses a principal name with hierarchical major and minor modifiers. Each sediment is given a principal name based upon the group to which it belongs. The groups are

1. The pelagic sediment group (>60% biogenic grains), which uses the following principal names to describe the composition and degree of consolidation of the sediment:
 - a. Ooze: unconsolidated calcareous and/or siliceous biogenic sediments;
 - b. Chalk: firm biogenic sediment composed predominantly of calcareous biogenic grains; and
 - c. Limestone: hard pelagic sediment composed predominantly of calcareous pelagic grains.
2. The mixed sediment group (40% to 60% biogenic grains).
3. The siliciclastic sediment group (<40% biogenic grains), which uses principal names to describe texture. Names are assigned according to the following guidelines:
 - a. The Udden-Wentworth grain-size scale (Wentworth, 1922) defines the textural groups that are used as the principal names of siliciclastic sediments. Biogenic components are not included in assigning the texture.
 - b. The sediment is placed in one of the groups shown in Figure 2 on the basis of the siliciclastic components alone. When two or more textural groups are present, the dominant component is listed as the principal name, and modifiers are assigned as major components. Other components are then assigned on a whole-sediment basis, and all major or minor components are included in the name in order of increasing abundance. It should be noted that this scheme can result in some components being included in the sediment name, although on a whole-sediment basis they do not quite comprise 10% of the sediment.
 - c. The suffix “stone” is affixed to the principal names sand, silt, and clay when the sediment is lithified.

Major and Minor Modifiers

The principal name is preceded by major modifiers and followed by minor modifiers (which are preceded by the term “with”) that de-

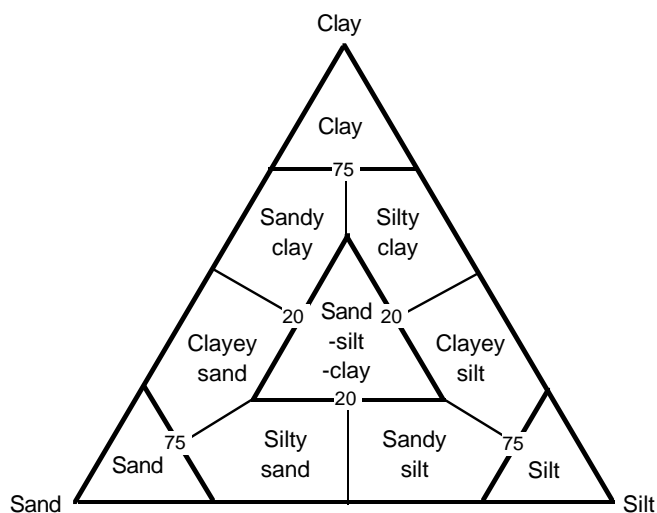


Figure 2. Ternary diagram used in the classification of siliciclastic sediments (modified after Shepard [1954]).

scribe the lithology of the granular sediment in greater detail. The most common use of major and minor modifiers is to describe the composition and texture of grain types that are present in major (>25%) and minor (10% to 25%) proportions. Modifiers are listed in order of increasing abundance. Some examples of unconsolidated sediments employing this classification scheme are as follows:

1. A sediment containing 30% clay, 15% foraminifers, and 55% nannofossils would be called a clayey nannofossil ooze with foraminifers.
2. A sediment with 4% foraminifers, 10% diatoms, 25% silt, 29% nannofossils, and 31% clay would be a silty nannofossil clay mixed sediment with diatoms.
3. A sediment with 10% sand, 26% silt, 30% clay, and 34% nannofossils would be a silty nannofossil clay with sand.

X-ray Diffraction

One sample from each core at one hole per site was chosen for X-ray diffraction analysis. Different holes at each site were sampled as necessary to provide an XRD profile to the depth cored. A limited number of additional samples was selected to characterize the mineralogy of representative lithological units. Bulk mineralogical analysis followed the procedure presented in the “Explanatory Notes” chapter of the *Initial Reports* volume for ODP Leg 171B (Shipboard Scientific Party, 1998), in which bulk samples were freeze-dried, ground, packed in sample holders, and scanned from 2° to 70° (2θ).

The results were analyzed with MacDiff software (MacDiff version 3.2b5 PPC, 1991–1996). The values presented in the data tables are relative percentages (based upon peak areas) for those components that were analyzed, and not for the sediment as a whole. Pyrite, hematite, aragonite, and, occasionally, alkali feldspar abundance estimates in particular may be overestimated because of interference by other mineral peaks.

Color Reflectance

A more detailed quantitative color and reflectance study was made with a Minolta spectrophotometer following the methods used during Leg 164 (Shipboard Scientific Party, 1996b). Sample intervals varied between 2 and 5 cm depending upon the resolution then being used by the MST. The color reflectance data (available on CD-ROM, back pocket, this volume) contain Munsell colors, $L^*/a^*/b^*$ color space values, and 400- to 700-nm color spectra values.

BIOSTRATIGRAPHY

Introduction

Preliminary age assignments were based on biostratigraphic analyses of calcareous nannofossils and planktonic foraminifers from core-catcher samples and samples from within the cores. We used the methods adopted during Leg 138 (Mayer, Pisias, Janecek, et al., 1992) and Leg 154 (Curry, Shackleton, Richter, et al., 1995) and, for those intervals that were multiply cored, we concentrated our efforts on the deepest of the three APC holes. In some cases, adjacent holes were correlated by locating the same biohorizons in each hole. This methodology, as opposed to just examination of core-catcher samples, enabled us to attain more precise shipboard stratigraphy. Constraint of calcareous nannofossil datums was achieved by examining one to six samples per section of core. Planktonic foraminifer datums were constrained to within one section (1.5 m) in the deepest hole of each site. Core-catcher sediments were not routinely examined for planktonic foraminifers in the other holes of a given site.

Age estimates of nannofossils and planktonic foraminifer biohorizons are reported in Tables 2 and 3. Ages for many of the biohorizons employed to construct the Leg 172 age model have been pub-

lished in the recent literature (e.g., Berggren et al., 1995a, 1995b), but the datum ages used on Leg 172 were derived from more recent time scales (e.g., the Leg 138 time scale of Shackleton et al. [1995] and the Leg 154 time scales of Tiedemann and Franz [1997] and Bickert et al. [1997]), which provide slightly different age estimates for several events. We updated and standardized the Pliocene–Pleistocene time scale to calibrate biohorizons, and converted the event ages to the astronomical time scale of Lourens et al. (1996). These ages do not differ significantly from those derived using the Pliocene–Pleistocene portion of the Cande and Kent (1995) time scale.

The chronostratigraphy and chronology of the time interval of interest (Pleistocene to early Pliocene) are considered generally well constrained, although some chronostratigraphic boundaries are not formally defined (e.g., the Pliocene/Miocene boundary). These boundaries are subjects of controversial discussions (see Berggren et al., 1995b). Because the Pleistocene chronostratigraphic terminology is in a state of flux, we adopted only the subseries subdivision (early, middle, and late Pleistocene). The base of the late Pleistocene has been considered equivalent to the base of marine isotope Stage (MIS) 5e. We used the record of magnetic susceptibility as a proxy for a stable isotope record. The base of the middle Pleistocene is generally considered to coincide with the onset of the Brunhes Chron. The Pleistocene/Pliocene boundary has been formally defined (see discussion in Berggren et al., 1995a), and is located near the top of the Olduvai (C2n) Magnetic Polarity Subchronozone with an estimated age of 1.806 Ma (Lourens et al., 1996).

We subdivided the Pliocene Series into the three standard stages: Gelasian, Piacenzian, and Zanclean. The Global Stratotype Section and Point (GSSP) of the base of the Gelasian Stage (upper Pliocene/middle Pliocene boundary) corresponds to MIS 103, and has an age of 2.589 Ma, close to the Matuyama/Gauss paleomagnetic boundary (Rio et al., 1994). The last appearance datums (LADs) of nannofossils *Discoaster pentaradiatus* and *D. surculus*, and the planktonic foraminifer *Globoconella puncticulata* are good approximations for the base of the Gelasian Stage. The GSSP of the base of the Piacenzian Stage (middle Pliocene/lower Pliocene boundary) corresponds to the Gauss/Gilbert paleomagnetic boundary (3.596 Ma; Lourens et al., 1996). The LADs of the nannofossil genus *Sphenolithus* (at 3.66 Ma; Fig. 3) and planktonic foraminifer *Hirsutella margaritae* (at 3.58 Ma; Fig. 3) and the beginning of the “Atlantic hiatus” of the planktonic

Table 2. Adopted calibrations and age estimates of calcareous nannofossil biohorizons.

Biohorizon	Biozone (base)		Adopted calibration (δ^{18} record or GPTS)	Adopted age (Ma)	Reference	Remarks
	(1)	(2)				
B <i>Acme Emiliana huxleyi</i>		NN21b	5a/5b	0.085	A	Diachronous between tropic-subtropical and transitional waters
B <i>Emiliana huxleyi</i>	CN15	NN21a	8	0.26	A	Isochronous
T <i>Pseudoemiliana lacunosa</i>	CN14b	NN20	12	0.46	A	Isochronous
Reent. medium <i>Gephyrocapsa</i> spp.	CN14a(?)		27	1	B	Diachronous—in Stages 29 (eastern equatorial Pacific), lower part of 25 (Atlantic, mid latitudes)
T large <i>Gephyrocapsa</i> spp.			37	1.24	C	Isochronous
T <i>Helicosphaera selli</i>			37/38 transition	1.25	C	Diachronous—in Stage 49 (eastern equatorial Pacific)
B large <i>Gephyrocapsa</i> spp.			55/56 transition	1.58	D	Diachronous—in Stage 48 (eastern equatorial Pacific)
T <i>Calcidiscus macintyre</i>			57/58 transition	1.67	C	Slightly diachronous—in Stage 55 (western equatorial Atlantic)
B medium <i>Gephyrocapsa</i> spp.	CN13b		59/60 transition	1.69	C	Isochronous
Pleistocene/Pliocene boundary			65	1.806	E	Formally defined at Vrica section
T <i>Discoaster brouweri</i>	CN13a	NN19	71/72 transition	1.95/1.97	C/F	Diachronous—in Stages 82/83 (eastern equatorial Pacific)
B <i>Acme Discoaster triradiatus</i>			82	2.15	C	
T <i>Discoaster pentaradiatus</i>	CN12d	NN18	100 (upper part)	2.52	F	
T <i>Discoaster surculus</i>	CN12c	NN17	100 (lower part)	2.53	F	
T <i>Discoaster tamalis</i>	CN12b		G11 (115)	2.83	F	
T <i>Sphenolithus</i> spp.	CN12aB			3.66	G	
T <i>Reticulofenestra pseudoumbilicus</i>	CN12aA	NN16	Within C2Ar (top Gilbert)	3.82	G	Isochronous
B <i>Ceratolithus acutus</i>			Within C3n.4n (Thvera)	5.05	H	
B <i>Ceratolithus rugosus</i>	CN10c	NN13	Within C3n.4n (Thvera)	5.1/5.23	H/F	
T <i>Triquetrorhabdulus rugosus</i>			C3n.4n “Thvera” (base)	5.23	H	
Pliocene/Miocene boundary			Within C3r	5.333	E	Not formally defined
B <i>Ceratolithus acutus</i>	CN10b		Within C3r	5.37	H	
T <i>Discoaster quinqueramus</i>	CN10a	NN12	C3r (lower part)	5.54	H	Isochronous

Notes: Biohorizon abbreviations: B = base, T = top. Reent. = reentrance of taxon into the record after an absence. Biozones: (1) = zonation of Okada and Bukry (1980); (2) = zonation of Martini (1971). GPTS = geomagnetic polarity time scale. Reference abbreviations: A = Thierstein et al. (1977), B = Raffi (unpubl. data), C = Raffi et al. (1993), D = Lourens et al. (in press), E = Lourens et al. (1996), F = Tiedemann et al. (1994), G = Raffi and Flores (1995), H = Backman and Raffi (1997).

Table 3. Age estimates of planktonic foraminifer biohorizons.

Biohorizon	Biozone (base)	Adopted age (Ma)	Reference
B <i>Globorotalia tumida flexuosa</i>		0.068	A
Reent. <i>Globorotalia tumida flexuosa</i>		0.401	A
Reent. <i>Truncorotalia crassiformis hessi</i>		0.075	A
T <i>Globigerinoides obliquus</i>		1.3	B
T <i>Globigerinoides fistulosus</i>	Pt1	1.77	A
Pleistocene/Pliocene boundary		1.806	C
B <i>Truncorotalia truncatulinoides</i>	N22	2.0	D
B (common) <i>Globoconella inflata</i>		2.16	E
T <i>Menardella exilis</i>		2.2 (2.15)	D (A)
T <i>Menardella miocenica</i>	PL6	2.3	D
Reent. <i>Pulleniatina</i> spp. (Atlantic)		2.3	D
T <i>Globoconella puncticulata</i>		2.41	A
T <i>Menardella pertensis</i>		2.6	B
T <i>Dentoglobigerina altispira</i>	PL5	3.12 (3.09)	D (A)
B <i>Globigerinoides fistulosus</i>		3.2	D
B <i>Truncorotalia tosaensis</i>	N21	3.2 (3.35)	D (A)
T <i>Pulleniatina</i> spp. (Atlantic)		3.5 (3.45)	D (A)
B <i>Menardella miocenica</i>		3.6 (3.55)	D (A)
T <i>Hirsutella margaritae</i>		3.58	D
D <i>Pulleniatina</i> (S to D coiling change)		4.0	D
T <i>Globoturborotalita neperthes</i>	PL2	4.27	A
Pliocene/Miocene boundary		5.33	C

Note: Biohorizon abbreviations: B = base, T = top, Reent. = reentrance of taxon into the record after an absence, S = sinistral, D = dextral. Reference abbreviations: A = Berggren et al. (1995b), B = Chaisson and Pearson (1997), C = Curry, Shackleton, Richter, et al. (1995), D = Chaisson and Leckie (1993), E = Weaver and Clement (1986). Ages in parentheses are drawn from Berggren et al. (1995b).

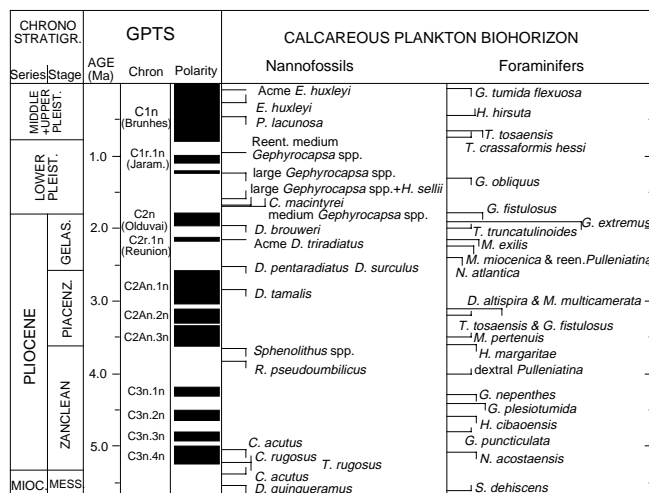


Figure 3. Adopted chronostratigraphy and calcareous plankton biochronology. Geomagnetic polarity time scale after Cande and Kent (1995), with revised ages after Hilgen et al. (1995) and Lourens et al. (1996).

foraminifer *Pulleniatina* spp. (3.5 Ma; Fig. 3) provide good approximations for the base of the Piacenzian Stage.

The GSSP of the base of the Zanclean Stage, the Pliocene/Miocene boundary, is not yet formally defined. Among contrasting proposals, we elect to recognize the boundary as corresponding to the re-establishment of open marine conditions in the Mediterranean after the Messinian salinity crisis at 5.333 Ma (Lourens et al., 1996). The calcareous nannofossil biohorizons that approximate the Pliocene/Miocene boundary are the first appearance datum (FAD) of *Ceratolithus acutus* (5.37 Ma), and the LADs of *Triquetrorhabdulus rugosus* (5.23 Ma) and *D. quinqueramus* (5.54 Ma).

Calcareous Nannofossils

During Leg 172, for biostratigraphic classification we referred to the biohorizons listed in Table 2, in which some of Martini's (1971) and Okada and Bukry's (1980) zonal markers are also indicated. We did not refer directly to the standard zonal schemes of Bukry (1973,

1975, code numbered by Okada and Bukry [1980]) and Martini (1971), because most of the biohorizons considered here are not associated with the standard zonal boundaries. In the Pleistocene interval at least nine biohorizons (four more than the standard ones) provide a highly resolved biostratigraphy. Moreover, some of the datum events used for zonal/subzonal definition in the two standard zonations are inadequately correlated to the oxygen isotope record or to the magnetostratigraphic record (particularly in the Pliocene interval), whereas others have taxonomic ambiguities that made questionable the placement of zonal boundaries. Most of the adopted calibrations of biohorizons are those obtained in the tropical and mid-latitude Atlantic in the reference sedimentary successions of Sites 607, 659, and 926 (see references in Table 2). Age assignments were provided by direct calibration to the oxygen isotope and magnetostratigraphic records.

Methods

Calcareous nannofossils were examined by means of standard light microscope techniques, under crossed nicols and transmitted light at 1200× magnification. For qualitative descriptions of calcareous nannofossil preservational states and estimation of relative abundances of the taxonomic categories, we have adopted the methodology used during Leg 154 (Curry, Shackleton, Richter, et al., 1995).

Planktonic Foraminifers

The tropical Neogene planktonic foraminifer "N-zonation" scheme referred to here follows Blow (1969), as modified by Kennet and Srinivasan (1983) and used on various recent ODP legs (e.g., Chaisson and Leckie, 1993; Chaisson and Pearson, 1997). However, the emphasis of the shipboard work will not be to establish a standard zonation, but rather to identify and constrain all available datums to within 1.5 m.

A list of planktonic foraminifer datums used in this study is presented in Table 3, which mainly follows Berggren et al. (1995a, 1995b) and Berggren et al. (1985) with various modifications (see Chaisson and Leckie, 1993; Chaisson and Pearson, 1997). Age estimates of planktonic foraminifer datums have been adjusted from earlier time scales to agree with the reversal ages assigned to the global polarity time scale by the orbitally tuned work of Lourens et al. (1996).

Methods

Unlithified ooze was either washed directly in tap water or soaked briefly in a weak (10%) hydrogen peroxide solution, then washed over a 63-µm mesh sieve. Semilithified ooze was first partially broken up by hand and then soaked in a weak hydrogen peroxide solution before washing and sieving. All samples were dried at approximately 50°C on a hot plate. In most samples only the >150-µm fraction was examined.

Benthic Foraminifers

Benthic foraminifers were identified in samples from Leg 172 to determine past changes in water-mass distribution. The taxa can be roughly divided into an Antarctic Bottom Water (AABW) assemblage, characterized by a high abundance of *Nuttallides umbonifera*, and a North Atlantic Deep Water (NADW) assemblage, characterized by high abundances of *Hoeglundina elegans*, *Cibicides wuellerstorfi*, and *Pyrgo* spp.

Methods

Sample preparation procedures were the same as those used for planktonic foraminifers. Benthic foraminifers were identified under the binocular microscope. Because several small species are impor-

tant indicators of water mass, the analyses were carried out on the >63- μm fraction. Benthic species abundance and preservation categories are those used by Curry, Shackleton, Richter, et al. (1995).

Diatoms

The diatom zonation used for this leg (Fig. 4) follows that of Baldauf and Pokras (1989). The original geographic location for which this zonation was used is not the same as that of this leg, but the overall scarcity of diatom biostratigraphic data for the mid-Atlantic leads to this decision. Diatoms were not present in all the cores at each site. They provide more depositional (and possibly environmental) than biostratigraphic information, but they can also provide another source of age dating along with nannofossils and planktonic foraminifers.

Methods

The smear slides made for nannofossil examination were also used to look for diatoms. When a sample was found to have abundant diatoms, it was sieved through a 20- μm screen in an attempt to remove some of the clays from the samples. Both sieved fractions were then examined at 1000 \times and 2000 \times .

PALEOMAGNETISM

Paleomagnetic studies conducted on the *JOIDES Resolution* during Leg 172 consisted predominantly of (1) long-core magnetic remanence measurements of archive-half sections before and after alternating field (AF) demagnetization and (2) magnetic remanence measurements of discrete samples collected from the working-half sections (typically one sample per core section) and stepwise AF demagnetized to 60 mT. The typical long-core demagnetization treatment applied to each section was selected based on the results of AF demagnetization experiments on discrete samples and on pilot archive-half sections.

Long-core remanence measurements and AF demagnetizations were performed using a long-core cryogenic magnetometer (2-G Model 760-R) with an in-line AF demagnetizer capable of reaching peak fields of 80 mT. During Leg 172 the archive halves were never demagnetized at peak fields greater than 60 mT.

The long-core magnetometer was also used to measure the remanence of discrete samples. The pass-through system can measure as many as 14 discrete samples per measurement cycle. We routinely ran seven samples per cycle to avoid possible effects from the response function of the magnetometer's pick-up coils that span nearly 20 cm. A few discrete samples from Site 1054 and 1055 were measured with a Molspin Minispin spinner magnetometer and the DTECH AF demagnetizer. The long-core magnetometer and the in-line AF demagnetization unit proved to be much more reliable and much faster than the spinner.

The magnetic susceptibility was measured for each whole-core section as part of the MST analyses. The MST susceptibility meter (a Bartington MS2C meter with an 88-mm coil diameter and a 0.565-kHz frequency) was set on SI units, and the values are stored in the JANUS database in raw meter units. To convert to true SI volume susceptibility values, these should be multiplied by 10^{-5} and then should be multiplied by a correction factor to take into account the volume of material that passed through the susceptibility coils. Except for measurements near the ends of each section, this factor for a standard ODP core is about 0.66 (=1/1.5). Within this volume, graphs illustrating MST susceptibilities are the raw unit values, with graph units typically labeled as 10^{-5} SI units. Susceptibilities for a few discrete samples were also measured on the Bartington susceptibility meter (Model MS2).

To investigate rock magnetic characteristics of discrete samples, anhysteretic remanent magnetization (ARM) and isothermal rema-

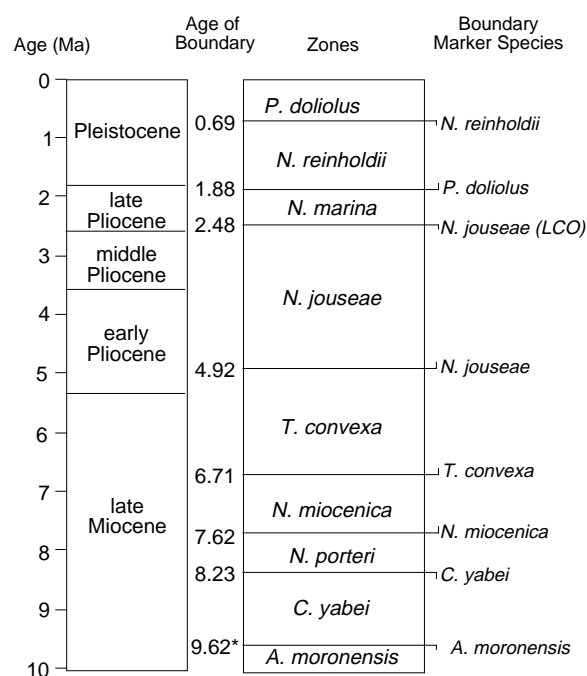


Figure 4. Diatom biostratigraphy and age estimates. Redrawn from Baldauf and Pokras (1989), and Baldauf (1984). Ages recalibrated to Hilgen et al. (1995) and Lourens et al. (1996) reversal ages. * = based on Shackleton and Crowhurst (1997). LCO = last common occurrence.

gent magnetization (IRM) experiments were also conducted. The DTECH demagnetizer was used to impart ARM to discrete samples. We imparted ARMs using a 150-mT alternating field and a 0.1-mT direct current field. We then progressively demagnetized the ARMs using the long-core system at 10-mT increments. IRMs were given to the discrete samples using the ASC Pulse magnetizer. IRM acquisition at fields of 50, 100, 200, 300, 400, 500, 750, 1000, and 1250 mT were measured and the stepwise AF demagnetized using the long-core system.

Details concerning the paleomagnetism laboratory, the operation of instruments, instrument sensitivity, core orientation, and other particulars can be found in the "Explanatory Notes" chapters of previous ODP *Initial Reports* volumes, particularly those from Legs 170 and 171B (Shipboard Scientific Party, 1997a, 1998). Exceptions include the use of a new version of the LONG-CORE software, which was installed during transit to our first site, and a new AF demagnetizer (DTECH model D2000), which was installed during the port call in Charleston, South Carolina.

Sampling

All data collected by the longcore magnetometer during this leg have an error that affects the declination values. To correct the data files on the CD-ROM (back pocket, this volume), the y-axis component of the magnetic moment and intensity should be multiplied by -1 . Similarly, the raw declination values should be corrected by multiplying by -1 . This correction does not affect the inclination or total field intensity values presented in the tables or figures.

We used a 5-cm sample interval for long-core remanence measurements starting 5 cm before the core segment top and ending as much as 5 cm after the core segment bottom. We avoided using the measurements within 5 cm from the ends of each section, although we saved these values for future studies that might wish to deconvolve the remanence signal.

Discrete samples used in pilot demagnetization studies were typically taken at an increment of one per core from one hole at each site

from Sites 1054–1059 and at an increment of one per section from one hole at each site from Sites 1060–1064. Occasionally, discrete samples were taken at smaller increments (as small as every 2.5 cm) to examine geomagnetic excursions, reversals, or other intervals of interest. All discrete samples were taken from soft sediment using oriented standard plastic boxes (6 cm³). In some cases, a stainless steel extruder was used to collect samples, in which case the orientation arrow for the sample is marked on the lid of the plastic cube. A second arrow is also present on the opposite face of the cube. These arrows always point uphole. Other cubes, collected by pressing the plastic cube directly into the sediment, have only a single arrow on the cube face opposite the lid.

Magnetostratigraphy

Where magnetic cleaning successfully isolates the primary component of remanence, paleomagnetic inclination and paleomagnetic declinations relative to magnetic north derived from the tensor tool are used to assign a magnetic polarity to the stratigraphic column. Interpretations of the magnetic polarity stratigraphy, with constraints from the biostratigraphic data, are presented in the site chapters. The revised time scale of Cande and Kent (1995) was used for Cenozoic polarity boundaries.

STRATIGRAPHIC CORRELATION

The recovery of continuous sedimentary sequences in APC-cored intervals was critical to the paleoceanographic and sedimentologic objectives of Leg 172. Drilling of multiple holes at each site ensured that intervals missing from one APC hole caused by core breaks or coring disturbance were recovered in an adjacent hole. During Leg 172, as on several previous ODP legs, continuity of recovery was confirmed by development of composite depth sections and splices. The methods used on Leg 172 were similar to those used to construct composite depth sections during Leg 138 (Hagelberg et al., 1992), Leg 154 (Shipboard Scientific Party, 1995), Leg 162 (Shipboard Scientific Party, 1996a), Leg 167 (Shipboard Scientific Party, 1997b), and Leg 171B (Shipboard Scientific Party, 1998). The “Explanatory Notes” chapters of these publications adequately describe the need for composite sections and spliced records and the overall approach taken to construct them on ODP legs.

Briefly, the overall approach follows the strategy of Hagelberg et al. (1992), who used GRAPE density, magnetic susceptibility, and digital reflectance data to document the exact correlation between cores from each of several holes at a particular site. The alignment of clearly correlated features from different holes inevitably necessitates depth-shifting cores. Commonly, material is found to be missing between successive cores, even where there is nominal 100% recovery. The end product of this depth shifting is a new depth scale (meters composite depth [mcd]) that has the advantage of representing continuity but the disadvantage of being longer than the distance actually cored (meters below seafloor [mbsf]). Typically, the length is expanded by about 10%, but the factor varies from ~5% to ~20%. The reason for this expansion is not fully understood, but gas expansion, decompression of the sediment (Moran, 1997), and distortion by the coring process are involved.

To obtain a meaningful representation of the whole section recovered, it is convenient to create a spliced record (Hagelberg et al., 1992) that is constructed by adding sequential intervals of core from any one of the holes recovered, proceeding down from the seafloor. Such a splice is useful both for providing a continuous record of the shipboard high-resolution records for time-series analysis and for providing a template that permits sampling the recovered sedimentary record from different holes at a site for shore-based analysis without wasting samples or analytical time.

A significant limitation of this approach is that because of drill-induced distortion (including gas voids), it is seldom possible to

line up all the prominent features in two cores by using a linear depth offset. It is convenient to choose to align one core to another at that point that will be used to cross over from one core to the other in completing the splice. If the relationship between samples in parallel holes must be known very precisely, it may be necessary post cruise to map the data for each section of each hole onto the splice, creating another depth scale that is not linearly related to curated depth at the centimeter to decimeter scale (Hagelberg et al., 1995). Such a scale should be used for special purposes, and great caution is required to avoid generating unnecessary confusion.

During Leg 172, the core integration was performed using SPLICER, a software package developed by Peter deMenocal and Ann Esmay in the ODP Borehole Research Group at Lamont-Doherty Earth Observatory (LDEO). The data sets used were MST magnetic susceptibility and GRAPE density data, and reflectance data from the Minolta color scanner. We made use of the L*, a*, and b* output of the Minolta color scanner in preference to reflectance from individual color channels. In some sections of cores, changes in lightness (generalized reflectance, characterized by the lightness L*) are useful for correlation while in other sections color changes (characterized by a* and/or b*) are more useful. Affine and splice tables appropriate for use in the Splicer computer program are available on CD-ROM (back pocket, this volume).

The use of a composite depth section dramatically improves the ability to correlate between sites and to describe changes in sedimentation rate, especially if biostratigraphy and magnetostratigraphy provide a dense network of precisely determined age control points. The resulting sedimentation rates (mcd/m.y.) are artificially high by about 10% as a result of the stretched mcd scale. Note that to the extent that expansion caused by rebound can explain the growth of the mcd scale with depth, mass fluxes would be correct when calculated using shipboard densities and sedimentation rates determined by the mcd scale. Uniform sediment expansion causes rebound and would result in an increase in porosity. However, if expansion is caused by numerous small-scale gas voids, shipboard densities may be more similar to in situ densities, because they come from less disturbed intervals, and correction from mcd to actual depth may be more important.

It is important for some applications to rescale depths on the mcd scale back to true depth below seafloor. For example, to simulate a seismic section using physical properties measured in cores it is vital that the composite depth be used so as to simulate the complete section, but this must be rescaled to true depths to correctly predict the depths of the reflectors in the sediment. In the ideal case, this rescaling can be done most simply by a linear transformation based on the ratio of mcd to mbsf over the full composite section (as suggested by Hagelberg et al. [1992]). However, at sites where there is significant expansion due to gas, the relationship between mcd and mbsf may not be constant over the full depth range. In this instance, linear transformations can be determined over different depth intervals where expansion appears constant. Also, at sites where a single hole penetrated a greater distance than other holes, it may be convenient to continue the composite depths and splice into the range where no true spliced record is possible. In this instance, there is only a constant offset between mcd and mbsf. A more complex procedure is to rescale on a core-by-core basis. This method was adopted for high-resolution conductivity measurements by the Leg 162 Shipboard Scientific Party (1996a; equations 20–22). Another method, possible when data are available from downhole logs, is to rescale the spliced record through alignment of MST data with downhole logs. In particular, both MST and downhole logs measure natural gamma radiation, which often has a distinctive signal that can be matched between cores and logs.

During Leg 172, one or more composite depth sections and spliced records were generated for each site, and the results are presented in the “Composite Depths and Stratigraphic Correlation” section of each site chapter. Three composite depth sections were determined for Site 1062, located on a mud wave, because different groups of holes sampled different wave flanks, and the sedimentary se-

quences were different enough that they could not be represented by a single spliced record. One composite depth section was determined for the other sites. Results include tables listing the applied offsets and the pieces used to make the spliced record. Downhole plots of magnetic susceptibility, GRAPE density, lightness (L^*), and the chromaticity variables (a^* and b^*) are also shown. These plots show each core plotted at its appropriate composite depth alongside the spliced record. In some cases, holes consisting of one or two cores are not plotted on these figures, although their offsets were determined and are available in the tables. Also marked on each plot are the depths at which the splice moves from one core to another. The spliced records for magnetic susceptibility, L^* , a^* , and b^* are also plotted in each chapter. Tables with the spliced data for each site and the composite depth information for each core are presented on CD-ROM (back pocket, this volume).

SEDIMENTATION AND MASS ACCUMULATION RATES

Shipboard sedimentation-rate calculations are important for preliminary stratigraphic and paleoceanographic interpretations and are useful for guiding postcruise sampling plans. To determine sedimentation rates on Leg 172, we first estimated an age/depth model from calcareous plankton biohorizons (for 0–4 Ma) and, if they were precisely determined, magnetic polarity reversals. Ages adopted for biohorizons are reported in Table 2 (see “Biostratigraphy” section, this chapter). The geomagnetic polarity time scale is that of Cande and Kent (1995) and Berggren et al. (1995b). At each site, magnetostratigraphic and biostratigraphic datums were tabulated and age/depth plots were made. We used linear interpolation between reliable datums to calculate sedimentation rates for each site in both the meters below seafloor and meters composite depth scales.

Sedimentation rates and age/depth models based on integrated biomagnetostratigraphy have a coarse resolution (10^5 yr) for time intervals spanned by the sedimentary sections recovered on Leg 172. These can be refined, particularly for the time interval from 0 to 900 ka, by making reference to the standard oxygen isotope stratigraphy (OIS), which provides a chronostratigraphic framework with a resolution of about 2×10^3 to 3×10^3 years (Imbrie et al., 1984). Although oxygen isotope data are unavailable on board the ship, most of the sediments recovered during Leg 172 show cyclic variations of lithologic and physical parameters that are obviously related to the same orbitally tuned climatic forcing that produces the oxygen isotope variability. Specifically, the variability in the magnetic susceptibility record at most sites shows a clear cyclicity that can be correlated for the past 900 k.y. to the stacked low-latitude oxygen isotope record of Bassinot et al. (1994) or to SPECMAP (a spectral mapping of stacked oxygen isotope records; Fig. 5). Therefore, using magnetic susceptibility as a proxy for the OIS, we have constructed high-resolution age/depth models for the interval from 0 to 900 ka for all Leg 172 sites, except Sites 1054 and 1064. These age models rely on accurately matching the dated oxygen isotope events (Martinson et al., 1987; Bassinot et al., 1994) with a similar series of features in the magnetic susceptibility records, and should therefore be used with caution.

The high-resolution age scale based on magnetic susceptibility signals is constructed in three steps:

1. To minimize the discrepancies associated with the comparison between magnetic susceptibility and oxygen isotope records, the magnetic susceptibility records of all sites were first compared with each other. We first subdivided the Blake-Bahama Outer Ridge sites into two groups (the Bermuda Rise Site 1063 is considered separately) based on their different magnetic signatures. For each of the two groups, a “reference” site was chosen, based on both the quality of sediment recovered and the time period represented. The magnetic susceptibility of each of the other sites in the group is correlated with the refer-

ence site, producing a depth-to-depth correlation that fits each magnetic susceptibility record onto the depth of the reference site. The reference sites are (a) Site 1056, which was used as the reference for Sites 1055 and 1057, and (b) Site 1061, which was used as the reference for Sites 1058, 1059, 1060, 1062.

2. Next, we dated the magnetic susceptibility record of each “reference” site by comparing it to the low-latitude oxygen isotope stack (Bassinot et al., 1994). The tie points that connect the magnetic susceptibility and oxygen isotope records are the same for the two reference sites (Table 4). To confirm, and in some cases improve, the location of tie points, the color reflectance record was also compared with the oxygen isotope record at some sites. Even using both the magnetic susceptibility and color reflectance records, it was still difficult to identify some of the major climatic features, such as MISs 13–15 or 17–18, at some of the sites.
3. The final step was to date the nonreference magnetic susceptibility records by comparing them with the reference site for each group. Sedimentation rates could then be calculated for all sites using linear interpolation between the predefined tie points. The resulting age model was verified by checking the position of the top of the *Pseudoemiliana lacunosa* range (within MIS 12, see “Biostratigraphy” section, this chapter) and the position of the Brunhes/Matuyama boundary (the youngest part of MIS 19, see Tauxe et al., 1996).

The meters composite depth scale was used to provide age/depth relationships for each site, because it splices together the meters below seafloor depths of different holes to account for between-core gaps in recovery. Consequently, this scale expands the mbsf depth scale by 5% to 20% (see “Stratigraphic Correlation” section, this chapter). The sedimentation rates obtained using the mcd scale are thus greater than those produced using mbsf depths.

The sedimentation rates are not corrected to account for the compaction of the sediment downhole. Using the porosity measurements (see “Physical Properties” section, this chapter), the compaction is estimated to be 50% in the longest holes at Sites 1061, 1062, and 1063.

Once the sedimentation rates are calculated, calcium carbonate and organic carbon accumulation rate (or flux) calculations are made for each site according to the relationship defined by van Andel (1975). Based on physical properties and sedimentation rate data,

$$MAR(TOC) = \frac{TOC}{100} \times LSR \times \left[WDB - 1.024x \left(\frac{Po}{100} \right) \right]$$

and

$$MAR(CaCO_3) = \frac{CaCO_3}{100} \times LSR \times \left[WDB - 1.024x \left(\frac{Po}{100} \right) \right],$$

where

MAR = mass accumulation rate ($g/cm^2/k.y.$),
 TOC = total organic carbon (wt%),
 $CaCO_3$ = calcium carbonate (wt%),
 LSR = linear sedimentation rate ($cm/k.y.$),
 WBD = wet bulk density (g/cm^3), and
 Po = porosity (%).

Because the sedimentation rate calculations are based on the mcd scale, a depth conversion from mbsf to mcd is done for wet bulk density, porosity, calcium carbonate, and organic carbon data. Then, a linear depth interpolation of physical properties data is made to approximate wet bulk density and porosity features of the sediment at the same depth as carbonate and organic carbon measurements were made.

The last step is the estimation of accumulation rates. Mean sedimentation rates are calculated within an age interval between the tie

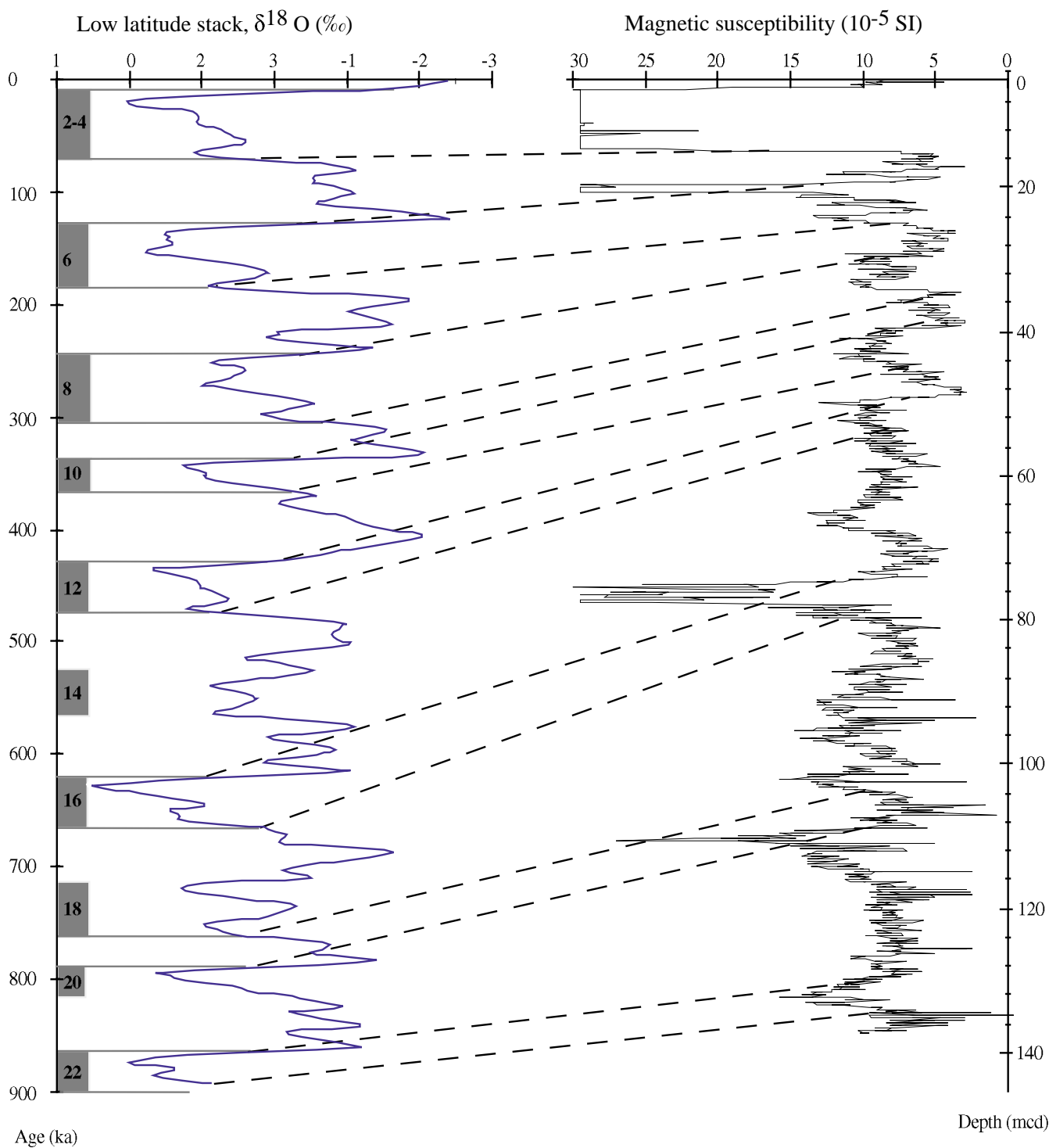


Figure 5. Correlation process between the low-latitude oxygen isotope stack (age reference) and the magnetic susceptibility record of Site 1056. The dashed lines indicate age/depth correlations based on their respective recognizable tie points.

points to the age reference record. We then calculated accumulation rates for each carbonate and organic carbon data point, wherever they were measured in the downhole sedimentary sections. We chose this method because carbonate and organic carbon observations were too sparse to give accurate mean values within a given time interval and, therefore, produce any reliable average accumulation rates. Thus, the results give only a rough estimate of the supply rate of carbonate and organic carbon to the sediment sink through time. However, this

method identifies significant oscillations through time that may be related to climatic variability.

GEOCHEMISTRY

Shipboard interstitial water analyses were performed on water squeezed from whole-round sections using Manheim (Manheim and

Table 4. Age-depth correlations, tie points used, and average sedimentation rates at reference Sites 1056 and 1061 and at Site 1063.

Site 1056				Site 1061				Site 1063			
Depth (mcd)	Nature of the tie point	Age (ka)	Average sed. rate (cm/k.y.)	Depth (mcd)	Nature of the tie point	Age (ka)	Average sed. rate (cm/k.y.)	Depth (mcd)	Nature of the tie point	Age (ka)	Average sed. rate (cm/k.y.)
0.14	HR	10		0.1	HR	10	47.12	0.12	HR	10	47.27
9.64	HR	70	15.83	28.37	HR	70	47.12	28.48	HR	70	47.27
14.59	HR	128	8.53	38.39	HR	128	17.28	35.96	HR	128	12.90
20.79	HR	188	10.33	54.77	HR	188	27.30	55.04	HR	188	31.80
24.04	HR	244	5.80	71.33	HR	244	29.57	65.14	HR	244	18.04
31.19	HR	302	12.33	84.55	HR	302	22.79	72.1	HR	302	12.00
34.39	HR	338	8.89	96.13	HR	338	32.17	76.39	HR	338	11.92
40.14	HR	364	22.12	100.71	HR	364	17.62	81.13	HR	364	18.23
44.29	HR	426	6.69	116.53	HR	426	25.52	94.75	HR	426	21.97
50.04	HR	476	11.50	124.11	HR	476	15.16	103.89	HR	476	18.28
69.34	HR	620	13.40	148.7	HR	620	17.08	123.1	HR	620	13.34
75.29	HR	672	11.44	152.88	HR	672	8.04	135.02	HR	672	22.92
99.43	HR	762	26.82	166.46	HR	762	15.09	149.32	HR	762	15.89
103.78	HR	788	16.73	175.06	HR	788	33.08	155.4	HR	788	23.38
111.28	HR	864	9.87	185.68	HR	864	13.97	166.21	HR	864	14.22
113.03	HR	900	4.86	195.45	HR	900	27.14	170.49	HR	900	11.89
114.58	BIOST.	1000	1.55	217.27	BIOST.	1000	21.82	205.4	MAGNET.	1070	20.54
147.13	BIOST.	1240	13.56	246.16	BIOST.	1240	12.04	326.18	MAGNET.	2140	11.29
170.38	BIOST.	1580	6.84	294.33	BIOST.	1580	14.17	376.3	MAGNET.	2581	11.37
				303.33	BIOST.	1670	10.00	415.3	BIOST.	3110	7.37
				306.61	BIOST.	1690	16.40				
				341.35	BIOST.	1960	12.87				
				363.61	BIOST.	2530	3.91				
				370.25	BIOST.	2830	2.21				

Note: HR = high-resolution tie point, defined between magnetic susceptibility record and the low latitude oxygen isotope stack; BIOST. = biostratigraphic tie point (see "Biostratigraphy" section, this chapter); MAGNET. = magnetostratigraphic tie point.

Sayles, 1974) and Reeburgh squeezers (Reeburgh, 1967). Sampling strategies and frequency differ for each site, so sampling specifics are given in separate site chapters. Chloride, salinity, alkalinity, pH, ammonium, phosphate, and silica were analyzed according to the methods described in ODP Technical Note 15 (Gieskes et al., 1991). Sulfate, potassium, calcium, and magnesium were analyzed by ion chromatography using a Dionex DX-100 ion chromatograph. Sodium was determined using charge balance calculations. Iron, manganese, and strontium of selected samples were analyzed by atomic absorption spectrophotometry using an air/acetylene flame. In the case of manganese and strontium analyses, lanthanum chloride solution was added as an ionization suppressor. The precision of each analysis is given in Table 5.

The shipboard organic geochemistry program included (1) monitoring of hydrocarbon gases; (2) measurement of sedimentary inorganic carbon; (3) elemental analysis of total carbon, total nitrogen, and total sulfur; and (4) characterization of organic matter by Rock-Eval pyrolysis. Standard ODP methods and instruments for sample collection and analyses are described by Kvenvolden and McDonald (1986) and in the "Explanatory Notes" chapter of the Leg 164 ODP *Initial Reports* volume (Paull, Matsumoto, Wallace, et al., 1996).

During Leg 172, the composition and concentration of hydrocarbons and other gases of the sediments were analyzed generally at intervals of one per core. Both headspace and gas-void sampling methods were used (Kvenvolden and McDonald, 1986). In addition, gases from selected samples were collected using Reeburgh squeezers (Reeburgh, 1967), which have the advantage of collecting interstitial waters and their associated gases from the identical whole-round section of core.

Low molecular-weight hydrocarbon samples were analyzed using a Hewlett-Packard (HP) 5890 II Plus gas chromatograph fitted with a flame ionization detector and a stainless steel column packed with HaySep S (80–100 mesh). When higher concentrations of C₂₊ hydrocarbons were present, gas samples were analyzed with the natural gas analyzer (NGA), which measures hydrocarbons from methane to heptane. This system consists of another HP 5890 gas chromatograph equipped with a HP-PLOT Al₂O₃ column with a 15 m × 0.53 mm × 15 m (film thickness) capillary tube. Helium was used as the carrier gas. Chromatographic responses were calibrated using commercial standards.

Table 5. Relative standard deviations of shipboard inorganic geochemical analyses.

Analysis	Analytical method	Reproducibility (1σ)	Standard
Alkalinity	Titration	2.1	IAPSO
pH	Titration	0.3	Orion standards
Cl ⁻	Titration	0.2	IAPSO
SO ₄ ²⁻	Ion chromatography	1.6	IAPSO
K ⁺	Ion chromatography	2.8	IAPSO
Mg ²⁺	Ion chromatography	2.1	IAPSO
Ca ²⁺	Ion chromatography	3.8	IAPSO
Sr ²⁺	Atomic absorption	<3	Standard curve (2.3-57 μM)
Mn ²⁺	Atomic absorption	<3	Standard curve (9-55 μM)
Fe ³⁺	Atomic absorption	<3	Standard curve (0.5-18 μM)
NH ₄ ⁺	Spectrophotometry	<6	Standard curve (0.5-30 mM)
PO ₄ ³⁻	Spectrophotometry	<5	Standard curve (0.2-10 μM)
H ₃ SiO ₄ ⁻	Spectrophotometry	<3	Standard curve (30-1500 μM)

Carbonate carbon concentrations were determined using a Coulometrics 5011 analyzer (Kvenvolden and McDonald, 1986). About 10 mg of freeze-dried, ground sediment was acidified with 2 M HCl. The liberated CO₂ was titrated with a blue methanolamine indicator. Carbonate contents were expressed as weight percent CaCO₃, assuming that all the carbonate was present as calcite.

Total carbon, nitrogen, and sulfur were determined using a Carlo Erba 1500 CNS analyzer (Kvenvolden and McDonald, 1986). Vanadium pentoxide was added to ~5 mg of freeze-dried, ground sediment and combusted at 1000°C in a stream of oxygen. The mixture of SO₂, CO₂, and N₂ was separated by gas chromatography, and measured using a thermal conductivity detector. TOC of sediment samples was determined by subtracting the amount of carbonate carbon from the total carbon values. Atomic organic matter C/N ratios were calculated from the TOC and total nitrogen concentrations.

Organic matter was evaluated by pyrolysis using the Delsi-Nermag Rock-Eval II system. This procedure uses a whole-rock pyrolysis technique to identify the type and the maturity of organic matter, as well as the petroleum potential of sediments (Espitalié et al., 1986). The Rock-Eval system involves a graduated temperature program that first heats the sediment sample to 300°C for 3 min, and then increases the temperature 25°C/min from 300° to 600°C. The initial heating purges volatile hydrocarbons (S₁) from the sediment; subse-

quent heating thermally cracks kerogen (S_2) within the sediment and releases higher molecular-weight hydrocarbons. The S_1 and S_2 hydrocarbons are measured with a flame ionization detector. During the S_2 program, the temperature that yields the maximum amount of hydrocarbons is called T_{max} , a parameter that assesses the maturity of sedimentary organic carbon. During the pyrolysis program, CO_2 released between 300° and 390°C from the thermal degradation of organic matter (S_3) is trapped and measured by a thermal conductivity detector. Rock-Eval II pyrolysis characterizes organic matter by allowing several parameters to be calculated: Hydrogen Index ($HI = 100 \times S_2/TOC$); Oxygen Index ($OI = 100 \times S_3/TOC$); Production Index [$PI = S_1/(S_1+S_2)$]; and Petroleum Potential [$0.083 \times (S_1+S_2)$]. Interpretation of Rock-Eval data is considered to be unreliable for samples containing less than 0.5% TOC (Peters, 1986).

PHYSICAL PROPERTIES

Introduction

The primary objective of Leg 172 was to provide a high-resolution, Pliocene and Pleistocene record of North Atlantic oceanographic variability from the continental slope to bathyal depths. With this objective in mind, the goals of the physical properties group were (1) to provide nearly continuous records of physical properties for (a) stratigraphic correlations between the different holes at one site, (b) producing complete composite sections, and (c) site-to-site comparisons; (2) to examine variations in physical properties that are related to the variations in sediment composition (thus, depositional history) on the Blake-Bahama Outer Ridge and Bermuda Rise; and (3) to provide data sets to aid in the interpretation of seismic reflection and downhole geophysical measurements.

Initial measurements of physical properties are undertaken on the MST. These measurements are performed on unsplit, 1.5-m-long sections and are nondestructive. The MST incorporates a GRAPE, a PWL, a magnetic susceptibility meter (MSM), and a natural gamma sensor (NGR). The MST provides a nearly continuous physical properties record; however, the quality of the data is highly dependent upon the condition of the core. Thermal conductivity, using the needle-probe method, was also measured at discrete intervals in whole-round sections.

Physical properties measurements made on split-core sections included undrained shear strength, longitudinal and transverse compressional wave velocity, and longitudinal and transverse resistivity. Index properties determined for discrete samples included dry bulk density, grain density, porosity, and void ratio. Usually, one to two index samples per section were taken, except where lithology or time dictated otherwise. Index samples were taken from the same position as the discrete velocity measurements. These measurements were usually made on the "A" hole. When time permitted, measurements of thermal conductivity (usually three per core), shear strength (one to two per section) and resistivity (two per section) were also made on the "A" hole; however, in some cases they were conducted at other holes.

The JANUS database for physical properties was fully operational on this leg. Physical properties data were transferred directly to the database from the computer systems controlling the MST and index properties sensors.

Laboratory Measurements

Index Properties

Index properties (bulk density, grain density, water content, porosity, dry density, and void ratio) were calculated from measurements of wet and dry masses and dry volumes. Samples of approximately 10 cm³ were taken for determination of index properties.

Sample mass was determined aboard ship to a precision of ± 0.01 g using a Scitech electronic balance. The sample mass was counter-

balanced by a known mass such that mass differences of usually 5 g were measured. Volumes were determined using a helium-displacement Quantachrome Penta-pycnometer. The pycnometer measures volumes to a precision of about ± 0.04 cm³. Sample volumes were repeated as many as three times until the last two measurements had <0.01% standard deviation. A purge time of 1 min was used before each run. A reference sphere of known volume was run with each group of four samples during all the measurements. The standard was rotated systematically among cells to check for errors.

Water content, bulk density, porosity, grain density, dry density, and void ratio were determined following the procedures outlined in Blum (1994). The procedures for the determination of these properties comply with the American Society for Testing and Materials (ASTM) designation (D) 2216 (ASTM, 1989). Bulk density, grain density, and porosity were computed from the wet and dry masses of the sample and dry volume was determined using "Method C" of Blum (1994).

Multisensor Track

The GRAPE device allows an estimation of wet bulk density by measuring the attenuation of gamma rays passing through the cores, where the degree of attenuation is proportional to density (Boyce, 1976; Gerland and Villinger, 1995). Calibration of the system was carried out using a known seawater/aluminum density standard with four components of different average densities. At Site 1062 it was found that the gamma calibration had not been carried out correctly at previous sites and that incorrect count rates had been assigned to the individual density components. Because this error was systematic, we were able to reassign the correct count rate per density component and recalculate the calibration function. The revised calibration functions for previous sites were applied to raw GRAPE data in the JANUS database, and the correct values are reported in this volume.

The PWL transmits a 500-kHz compressional wave pulse through the core at a rate of 1 kHz. The transmitting and receiving transducers are aligned perpendicular to the core axis. A pair of displacement transducers monitors the separation between the compressional wave transducers, so that variations in the outside diameter of the liner do not degrade the accuracy of the velocities. Where there is no acoustic coupling between the sediment and the liner, the PWL does not provide accurate velocity values and therefore is most useful in undisturbed APC cores. Initially, all *P*-wave data were accepted; however, it was not possible to edit the data in the JANUS database because signal amplitude data were not recorded. From Site 1055 onward, weak returns with signal strengths below a threshold value of 100 digital increments (out of a maximum of 255) were removed. Measurements were taken at either 2-, 4-, or 5-cm intervals, depending on the amount of time available. Calibration of the displacement transducer and measurement of electronic delay within the PWL circuitry was carried out using a series of acrylic blocks of known thickness and *P*-wave traveltime. The validity of the calibration was checked by measuring the *P*-wave velocity through a section filled with distilled water. Abnormally high PWL velocity measurements were noted at the beginning and end of each section. This was attributed to the PWL transducers measuring the velocity through the end cap. Thus, care should be taken in using the PWL data without removing these spurious values first.

Whole-core magnetic susceptibility was measured on a Bartington MS2C meter with an 80-mm (internal diameter) loop sensor at either 2-, 4-, or 5-cm intervals using the 1.0 (1 s integration time) range and averaging five readings. Susceptibility values were archived in raw instrument units (SI), which require multiplication by 6.6×10^{-6} to convert to volume-normalized SI units.

Natural gamma-ray emission was not routinely measured because of time constraints imposed by the high recovery rate. NGR was recorded on selected holes at 50-cm intervals in each section. The area of influence for the four NGR sensors is about ± 10 cm from the points

of measurements along the core axis. The installation and operating principles of the NGR system used on the *JOIDES Resolution* are discussed by Hoppie et al. (1994). Two of the four sensors used during Leg 172 had been replaced after Leg 171B. Data from 2048 energy channels were collected and archived. Counts have been summed up over the range from 200 to 3000 keV (in five windows), so as to be comparable with data collected during previous legs. This integration range also allows direct comparison with downhole logging data, which are collected over a similar integration range (Hoppie et al., 1994). Over the 200 to 3000 keV integration range, background counts measured using a core liner filled with distilled water averaged 18 per 30-s measurement period. No corrections were made to XCB core NGR data to account for sediment incompletely filling the core liner. Before starting measurements, the four sensor gains were adjusted so that the combined potassium peak was as sharp as the individual peaks when the other three were disabled. The multichannel analyzer was then calibrated by assigning certain channels to the characteristic energies of ^{40}K and the main peak of ^{232}Th (Ocean Drilling Program, 1996).

The accuracy of GRAPE, PWL, and MSM measurements degrades considerably in APC and XCB sections with gas voids or where the core otherwise does not fill the liner completely or is disturbed. However, the general downhole trends can be used for stratigraphic correlation. Tables of all MST data can be found on CD-ROM in the back pocket of this volume.

Velocimetry

In addition to the velocity measurements with the PWL, compressional wave velocity was measured on split-core sections with the digital sound velocimeter (DSV) using two types of piezoelectric transducer pairs. The transducers were inserted into soft sediments along (z-direction) and orthogonal (y-direction) to the core axis. Velocity calculation is based on the fixed distance between the transducers (7 and 3.5 cm, respectively), measurement of the traveltime of an impulsive acoustic signal, and a delay constant determined by measuring a water standard. Periodically, the separation was precisely evaluated by running a calibration procedure in distilled water. A value of sound velocity in distilled water is determined (based on standard equations) for the measured temperature, with the computer calculating the transducer separation using the signal traveltime. Use of the DSV was stopped in more indurated sediments when sediment started to crack during insertion of the transducers. In this case a modified Hamilton frame velocimeter was used, which measured the traveltime of a 500-kHz signal orthogonally across the split-core section and core liner (x-direction). Orientation of the x, y, and z directions is indicated in Shipboard Scientific Party (1996a; fig. 8.). Sample thickness was measured directly from the velocimeter-frame lead screw through a linear-resistor output to a digital multimeter. Zero traveltimes for the velocity transducers were estimated by linear regression of traveltime vs. distance for a series of aluminum and lucite standards. Velocity data recorded in the JANUS database are uncorrected for in situ temperature and pressure. However, these corrections can be made using the relationships in Wylie et al. (1956), Wilson (1960), and Mackenzie (1981).

Undrained Shear Strength

The undrained shear strength S_u of the sediment was determined using the ODP motorized miniature vane shear device following the procedures of Boyce (1977). The vane rotation rate was set to 90°/min. Measurements were made only in the fine-grained, soft to very stiff units. A range of springs of various strengths were available; B-1, B-2, and B-4 springs were used during this leg. These springs were calibrated before the start of the leg. The instrument measures the torque and strain at the vane shaft using a torque transducer and potentiometer, respectively. The shear strength reported is the peak

strength determined from the torque vs. strain plot. In addition to the peak shear strength, the residual strength was determined from the same plot where the failure was not dominated by cracking of the sample (Pyle, 1984).

In the analysis of vane tests the assumption is made that a cylinder of sediment is uniformly sheared around the axis of the vane in an undrained condition, with cohesion as the principal contributor to shear strength. Departures from this assumption include progressive cracking within and outside the failing specimen, uplift of the failing core cylinder, drainage of local pore pressures (i.e., the test can no longer be considered to be undrained), and stick-slip behavior. Evidence of cracking was noted in the comments section of the results file. When this condition occurred, a pocket penetrometer was used to estimate the shear strength of the sediment. The initial penetrometer measurements were converted from kg/cm² to kPa and then divided by two as the penetrometer was calibrated as an unconfined compression test (for the ideal clay) equal to twice the undrained shear strength (Holtz and Kovacs, 1981).

Electrical Resistivity

The Wayne-Kerr Precision Component Analyzer was used to measure resistivity with a four-electrode method in which two outer electrodes inject an alternating current while two inner electrodes measure the resulting potential difference. The apparent resistance U/I is proportional to the resistivity of the medium. The probes used on this leg consisted of four needles (Wenner array) spaced at 10-mm intervals. Electrical resistivity was usually measured about twice per section in one hole, per site. A number of measurements were made both in longitudinal and transverse directions to evaluate the anisotropy.

Calibration was done with standard seawater, where the area/length parameter of the probe is determined as the ratio of known resistance of seawater at a given temperature to that measured by the probe. The area/length parameter was measured in both the longitudinal (z) and transverse (y) directions. In practice, obtaining and maintaining the correct fluid level in the calibration bath proved difficult because the electrodes should be inserted in the calibration bath at the same level as they would be in sediment. To achieve this, the upper ends of the electrodes (not inserted into the sediment) were covered with silicon sealant to allow the probe to be submerged in the calibration bath. The area/length function was determined as 0.0787 for the z direction and 0.0826 for the y direction.

Thermal Conductivity

The thermal conductivity of cored material was measured using the needle-probe method, in full-space configuration for soft sediments (von Herzen and Maxwell, 1959). Measurements were taken using a single-probe TeKa (Berlin) TK-04 unit after the cores had equilibrated to the laboratory temperature. Data are reported in units of W/(m·K), and have an estimated error of 5%–10%.

A needle probe (#V00594) containing a heater wire and a calibrated thermistor was inserted into the sediment through a small hole usually drilled in the core liner 0.5 m from the top of each section before the section was split. At the beginning of each test, temperatures in the samples were monitored without applying a heater current until the background thermal drift was determined to be less than 0.04°C/min. Once the samples were equilibrated, the heater circuit was closed and the temperature rise in the probes was recorded. Thermal conductivities were calculated from the rate at which the temperature rose while the heater current was flowing.

Temperatures recorded during a time interval of 150 s were fitted with the least-squares technique to the appropriate equation:

$$T(t) = (q/4\pi k) \times \ln(t) + L(t),$$

where k is the apparent thermal conductivity, T is temperature, t is time, and q is the heat input per unit length of wire per unit time. The term $L(t)$ describes a linear change in temperature with time, and includes the background temperature drift and any linearity that results from instrumental errors and the geometrical inadequacies of the experiment. These inadequacies include the finite length of the probe and sample. All full-space measurements were corrected for a linear offset between measured and true thermal conductivities determined from a series of tests with standards of known conductivities.

DOWNHOLE LOGGING

Introduction

Downhole logs are used to determine physical, chemical, and structural properties of formations penetrated by drilling, thereby complementing discrete core measurements. The data are rapidly collected and interpretation of the continuous in situ measurements allows stratigraphic, lithologic, geophysical, and mineralogic characteristics of the formation to be quantified. When core recovery is incomplete, log data may serve as a proxy for physical properties and sedimentological data and permit the core to be placed in its proper stratigraphic position within the cored interval. Geophysical well logging is also used to aid in characterization of lithologic sequences when integrated with core and seismic reflection data.

Examples of the use of downhole logs for paleoceanographic objectives are given in the ODP Leg 167 *Initial Reports* volume (Lyle, Koizumi, Richter, et al., 1997) and for gas hydrate objectives (where in situ information is of paramount importance) in the ODP Leg 164 *Initial Reports* volume (Paull, Matsumoto, Wallace, et al., 1996)

Holes 1061A and 1063A were logged during Leg 172. The triple combination and Formation MicroScanner (FMS-Sonic) logging tool strings (see Table 6) were run in each hole.

Principles and Uses of the Tools

The principle of operation and uses of the tools are described in Serra (1984, 1986) and Rider (1996). They are briefly summarized below.

The natural gamma-ray tool (NGT) and hostile environment natural gamma-ray sonde (HNGS) measure the natural gamma radiation from isotopes of potassium (K), thorium (Th), and uranium (U) in the sediment surrounding the tool. High K and Th values indicate greater clay concentrations, and increased U values often indicate the presence of organic matter.

The accelerator porosity sonde (APS) emits fast neutrons, which are slowed by hydrogen in the formation, and the energy of the rebounded neutrons is measured. Most hydrogen is in the pore water; hence, porosity may be derived. However, hydrogen bound in minerals such as clays also contributes to the measurement, so the raw porosity value is often overestimated.

The hostile environment litho-density tool (HLDT) emits high-energy gamma rays, which are scattered by the electrons in the formation. The electron density (and hence the bulk density) is derived from the energy of the returning gamma rays. Porosity may also be derived from bulk density, if the matrix density is known. In addition, the photoelectric effect (PEF) is measured, and this varies according to the chemical composition of the sediment. The HLDT, APS, and HNGS were first used by the ODP during Leg 166 (Eberli, Swart, Malone, et al., 1997).

The dual-induction tool (DIT) measures the formation resistivity at three different penetration depths, by electromagnetic induction for the deep and medium resistivity and by current balancing for the shallow resistivity. Porosity, clay content, fluid salinity, grain size, and gas hydrate content all contribute to the resistivity. The sonic digital tool (SDT) measures the traveltimes of sound waves along the borehole wall between two transmitters and two receivers over distances of 2.4, 3.0, and 3.6 m.

The sonic velocity increases with consolidation, lithification, and gas hydrate content. An impedance log was produced from the density and sonic logs and related to the seismic survey sections, for example to investigate the acoustic transition at ~300 ms at Site 1063.

The FMS produces high-resolution images of the microresistivity character of the borehole wall. The tool comprises four orthogonal pads, each having 16 button electrodes that are pressed against the borehole wall (Serra, 1989). Roughly 30% of a 25-cm-diameter borehole is imaged. The vertical resolution is ~5 mm—features such as burrows, thin beds, fractures and veins can be imaged. The images are oriented, so that directional structure can be obtained for the sediment fabric.

Data Quality

Data quality is largely determined by the state of the borehole wall. If it is irregular, wide, or has many washouts, there may be problems with those tools that require good contact with the wall (density, porosity, and FMS). Deep-investigation measurements such as the resistivity and sonic velocity are least sensitive to borehole conditions. The quality of the borehole is helped by minimizing the circulation of drilling fluid and logging a young hole or a dedicated hole that has been drilled immediately before logging.

Operations

After the logging hole is cored, it is filled with viscous drilling fluid, and the drill pipe tripped to ~90 mbsf, back to the full depth, and then back to ~90 mbsf, to clean the hole and stabilize the borehole walls. Two tool strings were run sequentially down each hole on wireline cable. A newly refurbished wireline heave compensator was used to minimize the effect of the ship's motion on the tool position.

Incoming data for each logging run were recorded on disk, and monitored in real time on the Schlumberger Maxis 500 logging computer. Data were transferred to shipboard computers for preliminary interpretation using Schlumberger's GeoFrame software package, and also beamed to the Lamont-Doherty Earth Observatory Borehole Research Group (LDEO-BRG) using the digital high-speed data link of the Inmarsat B satellite communication system.

The LDEO-BRG, Leicester University Borehole Research (LUBR), and the Institut Méditerranéen de Technologie (IMT), in conjunction with Schlumberger Well Logging Services, provided the geophysical well logging aboard the *JOIDES Resolution*.

SITE GEOPHYSICS

Introduction

Site selection for Leg 172 was based on pre-site gravity and piston cores, 3.5-kHz data, and, in some cases, rather dated seismic profiles that were not always over the intended drill sites. For this reason, the ODP Site Survey Panel requested that high-resolution seismic surveys be conducted over all sites drilled during Leg 172. We also conducted an additional site survey for the purpose of proposing a new site in the Sohm Abyssal Plain. In total, we completed eight seismic surveys, which include profiles over all 11 sites (Table 7).

Site surveys typically consisted of using a generator-injector (GI) air gun, which was kindly loaned to ODP by Seismic Systems, Inc., and a Teledyne single-channel oil-filled streamer. A new six-channel seismic streamer produced by Innovative Transducers Incorporated was tested. Also, we compared the results from the GI gun to that of the 80-in³ water gun, which was run for a short segment of one survey. Lot positions at sites included a correction for the seismic reflection point being 230 m aft of the drill floor, the position of the GPS receiver.

The seismic data from each shot were sampled every 1 ms for 8 s and were digitally recorded on a Sun Sparcstation 10 in SEGY format, using the "a2d" acquisition package after application of an anti-

Table 6. Specifications of the downhole tools deployed during Leg 172.

Tool string	Tool	Measurement	Sample interval (cm)	Approximate vertical resolution (cm)
Triple combination (total length ~32 m)	HNGS	Natural gamma	15	45
	APS	Porosity	5 or 15	30
	HLDT	Bulk density, PEF	2.5 or 15	15/45
	DIT	Resistivity	2.5 or 15	200/150/75
	Temperature tool	Temperature	1 per second	—
FMS-Sonic (total length ~26 m)	NGT	Natural gamma	15	45
	SDT	Sonic velocity	15	120
	FMS	Resistivity image	0.25	0.5

Note: HNGS = hostile environment natural gamma-ray sonde, APS = accelerator porosity sonde, HLDT = hostile environment litho-density tool, DIT = dual-induction tool, NGT = natural gamma-ray tool, SDT = sonic digital tool, FMS = Formation MicroScanner.

Table 7. Summary of seismic lines and site crossings, Leg 172.

Seismic line	Start time	Shot point	End time	Shot point	Site or holes	Time at site*	Shot point at site†
1	19 February 1997, 14:38:12	1	19 February 1997, 22:30:24	3535	1054	22:00:05	3319
					1054	21:40:58	3174
					1055	19:44:47	2305
2	23 February 1997, 18:12:43	1	24 February 1997, 00:11:15	2372	1055	19:20:12	2121
					1056	19:00:58	342
					1056	19:38:14	591
3	27 February 1997, 22:52:03	1	28 February 1997, 01:33:34	1071	1057	23:18:30	2055
					1058	00:06:15	502
					1058	01:24:14	1018
4	6 March 1997, 01:01:01	6	6 March 1997, 03:15:25	891	1059	00:15:25	563
					1059	00:54:02	818
					1060	01:31:49	218
5	8 March 1997, 14:44:16	1	8 March 1997, 17:52:49	1028	1061	17:25:15	885
					1061	16:13:27	493
					1062A-1062D	11:54:00	210
6	14 March 1997, 11:13:23	1	14 March 1997, 14:29:23	979	1062A-1062D	14:09:27	887
					1062E-1062F	11:59:35	238
					1062E-1062F	13:37:59	725
					1062G-1062H	11:55:35	218
					1064	19:12:25	972
7	24 March 1997, 15:42:57	1	24 March 1997, 19:29:59	1047	1063	03:18:31	187
					1063	03:58:01	368
					1063	03:58:01	368
8	25 March 1997, 02:39:28	1	25 March 1997, 04:08:38	412	1063	03:58:01	368

Note: * = times for all site crossings (first time is primary crossing); † = shot point at site corrected for streamer length.

aliasing filter with a corner frequency at 250 Hz. Seismic data were copied to both 4-mm and 8-mm digital tapes after the site survey. Seismic data were processed using the SIOSEIS software package (Paul Henkart, Scripps Institute of Oceanography), and displayed on a HP 650C "Design Jet" plotter. Processing of SCS GI gun data included water-bottom mute, band-pass filter, deconvolution, and automatic gain control (AGC). Gray-scale images of the processed seismic data crossing each site were created using a program written on board ship and used in core-seismic integration. A sediment sound velocity profile was determined prior to the cruise based on vertical seismic profiles (VSP) acquired on Leg 164 (Paull, Matsumoto, Wallace, et al., 1996). The simplified velocity profile (linear from 1.5 km/s at the sediment surface to 1.8 km/s at 500 m subbottom) was used to create a time-depth table which was used for preliminary correlation between seismic profiles and the cored section (Table 8). Preliminary evaluation of Leg 172 velocity log data at Sites 1061 and 1063 suggests that Table 8 depths are correct to within ~10 m.

Two high-frequency echo-sounders (precision depth recorders [PDR]), running at 3.5 and 12 kHz, respectively, were used to acquire bathymetric data as well as high-resolution reflection records of the uppermost sediment layers. These profilers were run whenever the ship was underway between sites. Data from both systems were recorded on Raytheon Model 1807M analog line scanning recorders, although the 12-kHz recorder failed early in the leg. Both the 3.5-kHz and the 12-kHz PDRs used a Raytheon CESP III correlator echo sounder processor driven by a Raytheon PTR105B transceiver with a 2-kW sonar transmitter. The 3.5- and 12-kHz PDRs each use a single EDO type 323c transducer. The transducers are mounted in a sonar dome on the hull, 45 m forward of the drill floor. This location was chosen to reduce ship-generated noise and signal attenuation from

aeration beneath the hull. Both recorders were annotated automatically at fixed intervals, usually every 0.5 hr. Depth readings were taken manually every 5 min and entered into an Excel spreadsheet. Only the 3.5-kHz data at Sites 1054, 1055, and 1063 were of sufficient quality to allow for correlation to the cored sediments.

Other onboard instrumentation used included a magnetometer (Geometrics Model G-886 proton precession magnetometer), which was run for most of the transit from the Sohm Abyssal Plain to Lisbon, and a global positioning satellite navigation system, which was used in differential mode for all except the Sohm Abyssal Plain and Bermuda Rise surveys. Magnetic data were recorded at 1-min intervals for the first part of the transit and then at 5-s intervals during the latter part.

REFERENCES

- ASTM, 1989. *Annual Book of ASTM Standards for Soil and Rock: Building Stones* (Vol. 4.08): *Geotextiles*: Philadelphia (Am. Soc. Testing and Mater.).
- Backman, J., and Raffi, I., 1997. Calibration of Miocene nannofossil events to orbitally tuned cyclostratigraphies from Ceara Rise. In Shackleton, N.J., Curry, W.B., Richter, C., and Bralower, T. (Eds.), *Proc. ODP, Sci. Results*, 154: College Station, TX (Ocean Drilling Program).
- Baldauf, J.G., 1984. Cenozoic diatom biostratigraphy and paleoceanography of the Rockall Plateau region, North Atlantic, Deep Sea Drilling Project Leg 81. In Roberts, D.G., Schnitker, D., et al., *Init. Repts. DSDP*, 81: Washington (U.S. Govt. Printing Office), 439–478.
- Baldauf, J.G., and Pokras, E.M., 1989. Diatom biostratigraphy of Leg 108 sediments: eastern tropical Atlantic Ocean. In Ruddiman, W., Sarnthein, M., et al., *Proc. ODP, Sci. Results*, 108: College Station, TX (Ocean Drilling Program), 23–34.

- Bassinot, F.C., Labeyrie, L.D., Vincent, E., Quidelleur, X., Shackleton, N.J., and Lancelot, Y., 1994. The astronomical theory of climate and the age of the Brunhes-Matuyama magnetic reversal. *Earth Planet. Sci. Lett.*, 126:91–108.
- Berggren, W.A., Hilgen, F.J., Langereis, C.G., Kent, D.V., Obradovich, J.D., Raffi, I., Raymo, M.E., and Shackleton, N.J., 1995b. Late Neogene chronology: new perspectives in high-resolution stratigraphy. *Geol. Soc. Am. Bull.*, 107:1272–1287.
- Berggren, W.A., Kent, D.V., Swisher, C.C., III, and Aubry, M.-P., 1995a. A revised Cenozoic geochronology and chronostratigraphy. In Berggren, W.A., Kent, D.V., Aubry, M.-P., and Hardenbol, J. (Eds.), *Geochronology, Time Scales and Global Stratigraphic Correlation*. Spec. Publ.—Soc. Econ. Paleontol. Mineral., 54:129–212.
- Berggren, W.A., Kent, D.V., and Van Couvering, J.A., 1985. The Neogene, Part 2. Neogene geochronology and chronostratigraphy. In Snelling, N.J. (Ed.), *The Chronology of the Geological Record*. Geol. Soc. London Mem., 10:211–260.
- Bickert, T., Curry, W.B., and Wefer, G., 1997. Late Pliocene to Holocene (2.6 to 0.0 Ma) western equatorial Atlantic deep water circulation: inferences from benthic stable isotopes. *ODP Leg 154*. In Shackleton, N.J., Curry, W.B., Richter, C., and Bralower, T.J. (Eds.), *Proc. ODP, Sci. Results*, 154: College Station, TX (Ocean Drilling Program).
- Blow, W.H., 1969. Late middle Eocene to Recent planktonic foraminiferal biostratigraphy. In Brönnimann, P., and Renz, H.H. (Eds.), *Proc. First Int. Conf. Planktonic Microfossils, Geneva, 1967*: Leiden (E.J. Brill), 1:199–422.
- Blum, P., 1994. *Index Properties: ODP Shipboard Laboratory Manual, Version 155*. College Station, TX (Ocean Drilling Program).
- Boyce, R.E., 1976. Definitions and laboratory techniques of compressional sound velocity parameters and wet-water content, wet-bulk density, and porosity parameters by gravimetric and gamma-ray attenuation techniques. In Schlanger, S.O., Jackson, E.D., et al., *Init. Repts. DSDP*, 33: Washington (U.S. Govt. Printing Office), 931–958.
- , 1977. Deep Sea Drilling Project procedures for shear strength measurement of clayey sediment using modified Wykeham Farrance laboratory vane apparatus. In Barker, P.F., Dalziel, I.W.D., et al., *Init. Repts. DSDP*, 36: Washington (U.S. Govt. Printing Office), 1059–1068.
- Bukry, D., 1973. Low-latitude coccolith biostratigraphic zonation. In Edgar, N.T., Saunders, J.B., et al., *Init. Repts. DSDP*, 15: Washington (U.S. Govt. Printing Office), 685–703.
- , 1975. Coccolith and silicoflagellate stratigraphy, northwestern Pacific Ocean, Deep Sea Drilling Project Leg 32. In Larson, R.L., Moberly, R., et al., *Init. Repts. DSDP*, 32: Washington (U.S. Govt. Printing Office), 677–701.
- Cande, S.C., and Kent, D.V., 1995. Revised calibration of the geomagnetic polarity timescale for the Late Cretaceous and Cenozoic. *J. Geophys. Res.*, 100:6093–6095.
- Chaisson, W.P., and Leckie, R.M., 1993. High-resolution Neogene planktonic foraminifer biostratigraphy of Site 806, Ontong Java Plateau (western equatorial Pacific). In Berger, W.H., Kroenke, L.W., Mayer, L.A., et al., *Proc. ODP, Sci. Results*, 130: College Station, TX (Ocean Drilling Program), 137–178.
- Chaisson, W.P., and Pearson, P.N., 1997. Planktonic foraminifer biostratigraphy at Site 925: Middle Miocene–Pleistocene (last 12 m.y.). In Shackleton, N.J., Curry, W.B., Richter, C., and Bralower, T.J. (Eds.), *Proc. ODP, Sci. Results*, 154: College Station, TX (Ocean Drilling Program).
- Curry, W.B., Shackleton, N.J., Richter, C., et al., 1995. *Proc. ODP, Init. Repts.*, 154: College Station, TX (Ocean Drilling Program).
- Eberli, G.P., Swart, P.K., Malone, M.J., et al., 1997. *Proc. ODP, Init. Repts.*, 166: College Station, TX (Ocean Drilling Program).
- Espitalié, J., Deroo, G., and Marquis, F., 1986. La pyrolyse Rock-Eval et ses applications, Partie III. *Rev. Inst. Fr. Pet.*, 41:73–89.
- Gerland, S., and Villinger, H., 1995. Nondestructive density determination on marine sediment cores from gamma-ray attenuation measurements. *Geo-Mar. Lett.*, 15:111–118.
- Gieskes, J.M., Gamo, T., and Brumsack, H., 1991. Chemical methods for interstitial water analysis aboard *JOIDES Resolution*. *ODP Tech. Note*, 15.
- Hagelberg, T., Shackleton, N., Pisias, N., and Shipboard Scientific Party, 1992. Development of composite depth sections for Sites 844 through 854. In Mayer, L., Pisias, N., Janecek, T., et al., *Proc. ODP, Init. Repts.*, 138 (Pt. 1): College Station, TX (Ocean Drilling Program), 79–85.
- Hagelberg, T.K., Pisias, N.G., Shackleton, N.J., Mix, A.C., and Harris, S., 1995. Refinement of a high-resolution, continuous sedimentary section for studying equatorial Pacific Ocean paleoceanography, Leg 138. In Pisias, N.G., Mayer, L.A., Janecek, T.R., Palmer-Julson, A., and van Andel, T.H. (Eds.), *Proc. ODP, Sci. Results*, 138: College Station, TX (Ocean Drilling Program), 31–46.
- Hilgen, F.J., Krijgsman, W., Langereis, C.G., Lourens, L.J., Santarelli, A., and Zachariasse, W.J., 1995. Extending the astronomical (polarity) time scale into the Miocene. *Earth Planet. Sci. Lett.*, 136: 495–510.
- Holtz, R.D., and Kovacs, W.D., 1981. *An Introduction to Geotechnical Engineering*: Englewood Cliffs, NJ (Prentice-Hall).
- Hoppie, B.W., Blum, P., and the Shipboard Scientific Party, 1994. Natural gamma-ray measurements on ODP cores: introduction to procedures with examples from Leg 150. In Mountain, G.S., Miller, K.G., Blum, P., et al., *Proc. ODP, Init. Repts.*, 150: College Station, TX (Ocean Drilling Program), 51–59.
- Imbrie, J., Hays, J.D., Martinson, D.G., McIntyre, A., Mix, A.C., Morley, J.J., Pisias, N.G., Prell, W.L., and Shackleton, N.J., 1984. The orbital theory of Pleistocene climate: support from a revised chronology of the marine $\delta^{18}\text{O}$ record. In Berger, A., Imbrie, J., Hays, J., Kukla, G., and Saltzman, B. (Eds.), *Milankovitch and Climate* (Pt. 1), NATO ASI Ser. C, Math Phys. Sci., 126: Dordrecht (D. Reidel), 269–305.
- Kennett, J.P., and Srinivasan, M.S., 1983. *Neogene Planktonic Foraminifera: A Phylogenetic Atlas*: Stroudsburg, PA (Hutchinson Ross).
- Kvenvolden, K.A., and McDonald, T.J., 1986. Organic geochemistry on the *JOIDES Resolution*—an assay. *ODP Tech. Note*, 6.
- Lourens, L.J., Antonarakou, A., Hilgen, F.J., Van Hoof, A.A.M., Vergnaud-Grazzini, C., and Zachariasse, W.J., 1996. Evaluation of the Plio-Pleistocene astronomical timescale. *Paleoceanography*, 11:391–413.
- Lourens, L.J., Hilgen, F.J., and Raffi, I., in press. Base of large *Gephyrocapsa* and astronomical calibration of early Pleistocene sapropels in Site 967 and Hole 969D: solving the chronology of the Vrica section (Calabria, Italy). In Robertson, A.H.F., Emeis, K.-C., Richter, C., and Camerlenghi, A. (Eds.), *Proc. ODP, Sci. Results*, 160: College Station, TX (Ocean Drilling Program).
- Lyle, M., Koizumi, I., Richter, C., et al., 1997. *Proc. ODP, Init. Repts.*, 167: College Station, TX (Ocean Drilling Program).
- Mackenzie, K.V., 1981. Nine-term equation for sound speed in the oceans. *J. Acoust. Soc. Am.*, 70:807–812.
- Manheim, F.T., and Sayles, F.L., 1974. Composition and origin of interstitial waters of marine sediments, based on deep sea drill cores. In Goldberg, E.D. (Ed.), *The Sea* (Vol. 5): *Marine Chemistry: The Sedimentary Cycle*: New York (Wiley), 527–568.
- Martini, E., 1971. Standard Tertiary and Quaternary calcareous nannoplankton zonation. In Farinacci, A. (Ed.), *Proc. 2nd Int. Conf. Planktonic Microfossils Roma: Rome* (Ed. Tecnosci.), 2:739–785.
- Martinson, D.G., Pisias, N.G., Hays, J.D., Imbrie, J., Moore, T.C., Jr., and Shackleton, N.J., 1987. Age dating and the orbital theory of the ice ages: development of a high-resolution 0 to 300,000-year chronostratigraphy. *Quat. Res.*, 27:1–29.
- Mayer, L., Pisias, N., Janecek, T., et al., 1992. *Proc. ODP, Init. Repts.*, 138 (Pts. 1 and 2): College Station, TX (Ocean Drilling Program).
- Mazzullo, J.M., Meyer, A., and Kidd, R.B., 1988. New sediment classification scheme for the Ocean Drilling Program. In Mazzullo, J., and Graham, A.G. (Eds.), *Handbook for Shipboard Sedimentologists*. ODP Tech. Note, 8:45–67.
- Moran, K., 1997. Elastic property corrections applied to Leg 154 sediment, Ceara Rise. In Shackleton, N.J., Curry, W.B., Richter, C., and Bralower, T.J. (Eds.), *Proc. ODP, Sci. Results*, 154: College Station, TX (Ocean Drilling Program), 151–155.
- Munsell Color Company, Inc., 1975. *Munsell Soil Color Charts*: Baltimore, MD (Munsell).
- Ocean Drilling Program, 1996. *Tech Help: a Reference for the Physical Properties Specialist*, Science Services Department, 170.
- Okada, H., and Bukry, D., 1980. Supplementary modification and introduction of code numbers to the low-latitude coccolith biostratigraphic zonation (Bukry, 1973; 1975). *Mar. Micropaleontol.*, 5:321–325.
- Paull, C.K., Matsumoto, R., Wallace, P.J., et al., 1996. *Proc. ODP, Init. Repts.*, 164: College Station, TX (Ocean Drilling Program).
- Peters, K.E., 1986. Guidelines for evaluating petroleum source rock using programmed pyrolysis. *AAPG Bull.*, 70:318–329.
- Pyle, M.R., 1984. Vane shear data on undrained residual strength. *J. Geotech. Engr. Div., Am. Soc. Civ. Eng.*, 110:543–547.
- Raffi, I., Backman, J., Rio, D., and Shackleton, N.J., 1993. Plio-Pleistocene nannofossil biostratigraphy and calibration to oxygen isotopes stratigraphies from Deep Sea Drilling Project Site 607 and Ocean Drilling Program Site 677. *Paleoceanography*, 8:387–408.
- Raffi, I., and Flores, J.-A., 1995. Pleistocene through Miocene calcareous nannofossils from eastern equatorial Pacific Ocean (Leg 138). In Pisias, N.G., Mayer, L.A., Janecek, T.R., Palmer-Julson, A., and van Andel, T.H.

- (Eds.), *Proc. ODP, Sci. Results*, 138: College Station, TX (Ocean Drilling Program), 233–286.
- Reeburgh, W.S., 1967. An improved interstitial water sampler. *Limnol. Oceanogr.*, 12:163–165.
- Rider, M., 1996. *The Geological Interpretation of Well Logs*: Caithness (Whittles Publishing).
- Rio, D., Sprovieri, R., and Di Stefano, E., 1994. The Gelasian stage: a proposal for a new chronostratigraphic unit of the Pliocene series. *Riv. Ital. Paleontol. Stratigr.*, 100:103–124.
- Rothwell, R.G., 1989. *Minerals and Mineraloids in Marine Sediments*: Amsterdam (Elsevier).
- Serra, O., 1984. *Fundamentals of Well-Log Interpretation* (Vol. 1): *The Acquisition of Logging Data*: Dev. Pet. Sci., 15A: Amsterdam (Elsevier).
- , 1986. *Fundamentals of Well-Log Interpretation* (Vol. 2): *The Interpretation of Logging Data*. Dev. Pet. Sci., 15B.
- , 1989. *Formation MicroScanner Image Interpretation*: Houston (Schlumberger Educ. Services), SMP-7028.
- Shackleton, N.J., and Crowhurst, S., 1997. Sediment fluxes based on an orbitally tuned time scale 5 Ma to 14 Ma, Site 926. In Curry, W.B., Shackleton, N.J., Richter, C., and Bralower, T. (eds.), *Proc. ODP, Sci. Results*, 154: College Station, TX (Ocean Drilling Program).
- Shackleton, N.J., Crowhurst, S., Hagelberg, T., Pisias, N.G., and Schneider, D.A., 1995. A new late Neogene time scale: application to Leg 138 sites. In Pisias, N.G., Mayer, L.A., Janecek, T.R., Palmer-Julson, A., and van Andel, T.H. (Eds.), *Proc. ODP, Sci. Results*, 138: College Station, TX (Ocean Drilling Program), 73–101.
- Shepard, F., 1954. Nomenclature based on sand-silt-clay ratios. *J. Sediment. Petrol.*, 24:151–158.
- Shipboard Scientific Party, 1995. Explanatory notes. In Curry, W.B., Shackleton, N.J., Richter, C., et al., *Proc. ODP, Init. Repts.*, 154: College Station, TX (Ocean Drilling Program), 11–38.
- , 1996a. Explanatory notes. In Jansen, E., Raymo, M.E., Blum, P., et al., *Proc. ODP, Init. Repts.*, 162: College Station, TX (Ocean Drilling Program), 21–45.
- , 1996b. Explanatory notes. In Paull, C.K., Matsumoto, R., Wallace, P.J., et al., *Proc. ODP, Init. Repts.*, 164: College Station, TX (Ocean Drilling Program), 13–41.
- , 1997a. Explanatory notes. In Kimura, G., Silver, E.A., Blum, P., et al., *Proc. ODP, Init. Repts.*, 170: College Station, TX (Ocean Drilling Program).
- , 1997b. Explanatory notes. In Lyle, M., Koizumi, I., Richter, C., et al., *Proc. ODP, Init. Repts.*, 167: College Station, TX (Ocean Drilling Program).
- , 1998. Explanatory notes. In Norris, R.D., Kroon, D., Klaus, A., et al., *Proc. ODP, Init. Repts.*, 171B: College Station, TX (Ocean Drilling Program).
- Sigurdsson, H., Leckie, R.M., Acton, G.D., et al., 1997. *Proc. ODP, Init. Repts.*, 165: College Station, TX (Ocean Drilling Program).
- Tauxe, L., Herbert, T., Shackleton, N.J., Kok, Y.S., 1996. Astronomical calibration of the Matuyama-Brunhes boundary: consequences for magnetic remanence acquisition in marine carbonates and the Asian loess sequences. *Earth Planet. Sci. Lett.*, 140:133–146.
- Thierstein, H.R., Geitzenauer, K., Molino, B., and Shackleton, N.J., 1977. Global synchronicity of late Quaternary coccolith datum levels: validation by oxygen isotopes. *Geology*, 5:400–404.
- Tiedemann, R., and Franz, S.-O., 1997. Deep-water circulation, chemistry, and terrigenous sediment supply in the equatorial Atlantic during the Pliocene, 3.3–2.6 and 5.0–4.5 Ma. In Curry, W.B., Shackleton, N.J., Richter, C., and Bralower, T. (Eds.), *Proc. ODP, Sci. Results*, 154: College Station, TX (Ocean Drilling Program), 299–318.
- Tiedemann, R., Sarnthein, M., and Shackleton, N.J., 1994. Astronomic timescale for the Pliocene Atlantic $\delta^{18}\text{O}$ and dust flux records of Ocean Drilling Program Site 659. *Paleoceanography*, 9:619–638.
- van Andel, T.H., Heath, G.R., and Moore, T.C., Jr., 1975. Cenozoic history and paleoceanography of the central equatorial Pacific Ocean: a regional synthesis of Deep Sea Drilling Project data. *Mem.—Geol. Soc. Am.*, 143.
- Von Herzen, R.P., and Maxwell, A.E., 1959. The measurement of thermal conductivity of deep-sea sediments by a needle-probe method. *J. Geophys. Res.*, 64:1557–1563.
- Weaver, P.P.E., and Clement, B.M., 1986. Synchronicity of Pliocene planktonic foraminiferal datums in the North Atlantic. *Mar. Micropaleontol.*, 10:295–307.
- Wentworth, C.K., 1922. A scale of grade and class terms of clastic sediments. *J. Geol.*, 30:377–392.
- Wilson, W.D., 1960. Speed of sound in seawater as a function of temperature, pressure and salinity. *J. Acoust. Soc. Am.*, 32:641–644.

Ms 172-102

Table 8. Preliminary relationship between two-way traveltime and sub-bottom depth for Leg 172.

Two-way traveltime (ms)	Depth (m)
0	0
10	8
20	15
30	23
40	30
50	38
60	45
70	53
80	61
90	69
100	76
110	84
120	92
130	100
140	107
150	115
160	123
170	131
180	139
190	147
200	155
210	163
220	171
230	179
240	187
250	195
260	203
270	212
280	220
290	228
300	236
310	245
320	253
330	261
340	269
350	278
360	286
370	295
380	303
390	312
400	320
410	329
420	337
430	346
440	354
450	363
460	371
470	380
480	389
490	398
500	406